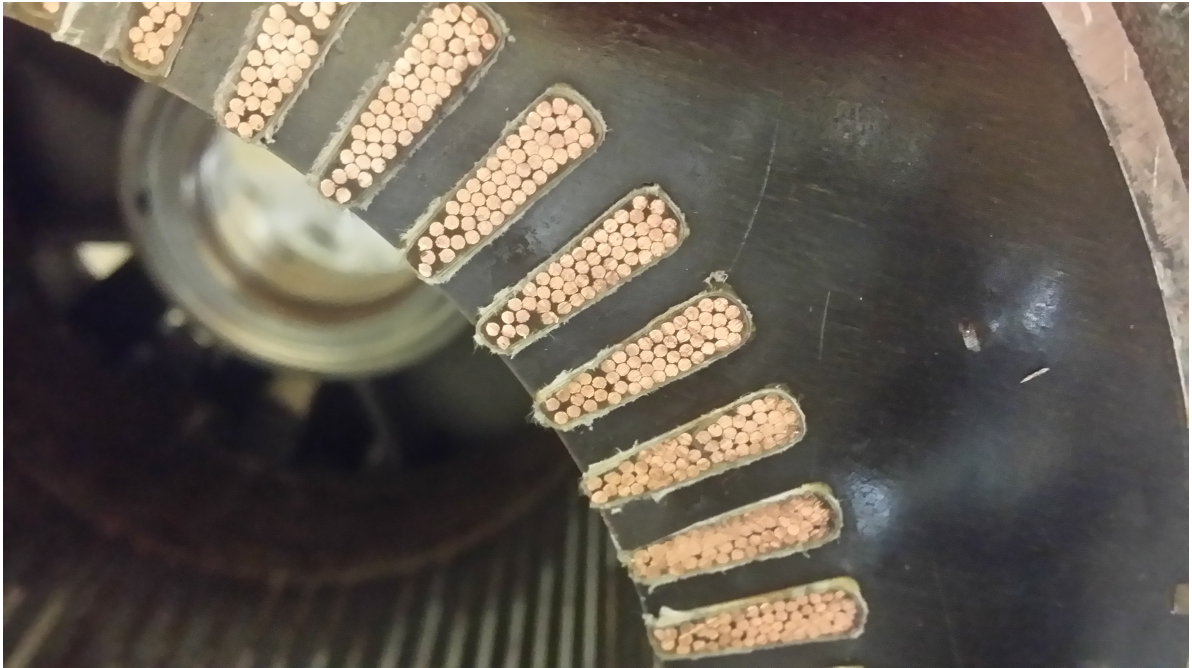# CHALMERS

UNIVERSITY OF TECHNOLOGY

Simulation of an Induction Machine for Electric Vehicle Purpose

Characterization and Modelling of a High Torque Density Induction Traction Machine

Master's Thesis

ERIC GÁMEZ SÁNCHEZ

TAPAS ANJAN SARANGI

Master's thesis

Simulation of an induction machine for electric vehicle purpose

ERIC GÁMEZ SÁNCHEZ
TAPAS ANJAN SARANGI

CHALMERS
UNIVERSITY OF TECHNOLOGY

Department of Electrical Engineering
Division of Electric Power Engineering
CHALMERS UNIVERSITY OF TECHNOLOGY
Gothenburg, Sweden 2017

Simulation of an induction machine for electric vehicle purpose

ERIC GÁMEZ SÁNCHEZ
TAPAS ANJAN SARANGI

Cover: Picture of cross section view of the stator of the machine modelled.

Simulation of an induction machine for electric vehicle purpose
Master's thesis
ERIC GÁMEZ SÁNCHEZ
TAPAS ANJAN SARANGI
Department of Electrical Engineering
Chalmers University of Technology

Abstract

In this thesis, a currently used on automotive induction machine is studied. A model with two different software programs is set up in order to understand its full behaviour. For creating the model of the machine, different tests were done on the machine in order to obtain all the necessary parameters. In addition, using a well known smaller machine, a model was set up on the two different software programs in order to understand the calculations and for having a base case to compare with the commercial one.

The results from the simulations in the two software and the measurements done on the machine were compared to validate the model. Some parameters matched well, as the powers, but others had some differences for variable working scenarios. The thesis resulted in different situations where the model can be used for a better understanding of the machine. In particular, the blocked rotor test was difficult to reproduce with one software.

Acknowledgements

We would like to thank especially to our supervisor Torbjörn Thiringer for the guidance during the development of this project. Without his support, our thesis would have never arrived to this point. Also, to all the colleagues and people from the department that somehow have helped us.

Moreover, we would like to thank our family and friends for the support given through all these months.

Contents

Contents

Abbreviations

BEV	Battery electric vehicle
EV	Electric vehicle
f	Frequency
FEA	Finite Element Analysis
FEM	Finite Element Method
FFT	Fast Fourier transform
I_0	Current trough stator's phase under no load conditions
I_r	Current drawn by the rotor
I_s	Current drawn by the stator
i_ϕ	Current representing the magnetizing branch and iron losses
I_{BR}	Current trough stator's phase under blocked rotor conditions
i_r	Current through the rotor
i_s	Current through one stator phase
ICE	Internal combustion engine
IM	Induction Machine
J	Inertia
LPM	Lumped Parameter Model
$maxwell$	Maxwell software
$MTPA$	Maximul torque per ampere
p	Pair of poles
P_f	friction losses
P_{Cu}	Copper losses on the stator
P_e	Electromagnetic power
P_{FE}	Iron losses
P_{Mec}	Mechanical losses
P_{rot}	Rotational losses
P_{st}	No-load stray losses and additional losses
PLL	Phase-locked loop

Contents

R_m Core loss resistance

R_r Rotor resistance

R_I Iron losses

R_r Rotor resistance

R_s Stator resistance

REM Rare earth metal

s Slip

T_e Electromagnetic torque

$TEFC$ Totally Enclosed Fan-Cooled

U_0 Stator's phase voltage under no load conditions

U_s Applied voltage to stator

U_{BR} Stator's phase voltage under blocked rotor conditions

u_s Phase voltage

X_m Magnetizing reactance

X_M Magnetizing inductance

X_r Rotor leakage inductance

X_s Stator leakage inductance

1
Introduction

1.1 Background

The first electric vehicle in history appeared in 1828, by the hand of Ányos Jedik. By 1900, 28 percent of cars in the USA were powered by electric propulsion systems. Despite their early emergence and expansion, internal combustion engines finally won the battle for being the main part of cars powertrain. Some of the reasons for this were the mass manufacturing, lead by Henry Ford, who made cars affordable, decreased petrol prices, thanks to the discovery of new reserves in the USA, the development of better ICE machines and the autonomy they offered, which was completely necessary to transverse non-urban areas. For these and other reasons, EV's did not reappear until the 1990s.

In 1990, EVs appeared again, and almost all of them have been powered with Permanent magnets DC brushless motors. There are only a few exceptions in recent years which have used AC motors, as it was considered inefficient and costly. One of these AC exceptions is the Tesla Model S machine. Although there are different versions of powertrain configurations, all of them have a three phase, four pole AC induction with a copper rotor machine. The most important fact is that Tesla Motors started to use it in a mass production, low-cost and with efficient manner which gave real challenge to the permanent magnets synchronous machine (PMSM) usage.

In this context, it is important to understand the full behaviour of these motors, especially the one used by Tesla, as it has been a revolution within full EV industry. Perhaps, industry will move towards this type of motors and more vehicles will start to use it. What is even more engaging, is to describe the energy losses that occur particularly in this motor. Only by having a better understanding of the efficiency, can it be well described and its success understood.

1.2 Society and Ethics

In a world, year after year, being more concerned about sustainability and human impact on the environment, this is a transverse subject that must be taken into account in every field. Especially in the transport sector, one of the current biggest sources of CO_2 generation. The increase of EV in society is interesting because it allows to reduce these emissions, if electricity generation comes from renewable energies, resulting in a more environmentally friendly way of developing the transport sector.

It is thus interesting to investigate these kind of motors due to the fact that they do not use rare earth metals (REM) in contrast to PMSM. These materials are scarce in nature. Furthermore, it is known that the extraction of this type of materials implies really bad conditions for human beings in undeveloped countries. Safety, health and human rights are matters that are often not accounted for whilst extracting them. Avoiding these materials, not only implies a better compromise with the environment, but also with society. [1]

1.3 Previous Work

The PMSM is the most used electric machine for vehicle applications starting from Toyota Prius until this date, but with the occurrence of Tesla Vehicles' the use of IM in the BEV sector has taken many by surprise. A lot of studies and projects have been developed about AC induction machines, since the first one appeared in 1888 developed by Nikola Tesla. Very little is known about the IM application into a BEV application. Missing data are a traction induction machines, about the efficiency of the machine, heat capacity of the construction material, obtainable MTPA curve etc.

1.4 Purpose

Accordingly, the main objective of this project is to understand a machine currently used in automotive sector by creating a model on a computer software to recreate different scenarios. Also, to determine and quantify how losses appear in a motor currently used in the industry, considering a steady-state scenario. A well known machine with experimental measurements and different studies is used [2] [3], machine A, to create the model in two different computer software. A traction induction machine is purchased by the university and referred to as machine B. The model of machine B is created from machine A model, making the necessary changes. Machine A is a 15 kW 6 pole induction machine squirrel cage from ABB, model MBL 180.

The specific objectives of the project are:

1. To quantify the parameters of the equivalent circuit of machine A and B, in order to simulate them.

2. To design and obtain a model with Maxwell and Motor-CAD for both machines.

2

Theory

2.1 Induction Machines

Induction machines are a type of device that can transform electric energy into mechanical rotating energy and vice versa. For the motor mode, they are developed in a way that, when an AC current is supplied through the fixed windings, a rotating magnetic field appears. And this, combined with the rotor structure allows for having a rotating shaft with an output torque.

2.1.1 Components

Generally, these machines have the following parts:
- Case: the enveloping of the whole motor used for the isolation and protection of internal pieces. As well, for avoiding damages to people.
- Rotor: rotating part of the machine that can be connected to the load.
- Stator: fixed part of the machine connected to the power supply. It is in charge of creating the inducted field into the rotor.
- Shaft: output of the motor connected to the rotor.
- Cooling System: in some cases it exists a cooling system to avoid high temperatures that could cause damages to the machine. Sometimes it consists of a fan attached to the back part of the shaft or a more complex system of liquid cooling through the rotor or stator.

2.1.1.1 Rotor

The rotor is the moving part of the machine, where the shaft is connected. For induction machines there are two possibilities of rotors, wound type or squirrel cage. The first one consists of a rotor made of windings, that can be connected to an outer circuit with brushes and slip rings. The possibility of setting the current allows to control the speed and torque of the motor, as it will be seen later on. Squirrel cage rotors consist of a structure made of bars and generally two short-circuit rings, one at each side, of either aluminum or copper. Between the bars, iron sheet laminations of another material is used. At the end, the bars work as a beam of windings coiled over the rotor and short circuited.

Moreover, the rotor can have different configurations. Taking into consideration the cage for the bars, it can happen that it has a large hole with two cavities for different bar shapes. This is called double cage rotor and increase the starting torque when the machine is grid connected.

Another possibility for the rotor bars is to make them in a way that are not parallel to the shaft so called skewing. In figure 2.1 can be seen how rotor bars can even have 2 skewing parts.

Figure 2.1: Example of a skewed rotor.

2.1.1.2 Stator

The stator of an induction machine is made of windings connected to a voltage source through a 3 phase system. It is the fixed part of the machine with a tubular shape surrounding the rotor and consequently the shaft. The windings go through the stator slots and can be placed in different layers. The end connection can be a wye or a delta connection, and in some cases changed for the starting process and normal operation.

2.1.2 Principle of Operation

2.1.3 Slip

The slip of an induction machine is defined as the parameter that determines the relative velocity between the rotor and the magnetic field. It is necessary that the value of the slip is different to 0, in order to have a torque. Otherwise, if the slip is 0, it means that the magnetic field applied to the rotor and its rotation are synchronized and therefore no current is induced into the rotor bars.

The equation that determines the slip is

$$s = \frac{(n_s - n)}{n_s} \cdot 100 \tag{2.1}$$

where the n_s is the speed of the magnetic field, synchronous speed, and n is the speed of the rotor. The rated value is usually between 1% and 7%, where the higher value is for smaller induction machines.

2.1.4 Equivalent Circuit

All machines can be described with an equivalent circuit, which can determine the performance with a few parameters. For an IM, in accordance to IEEE, the scheme is as presented in Figure 2.2.
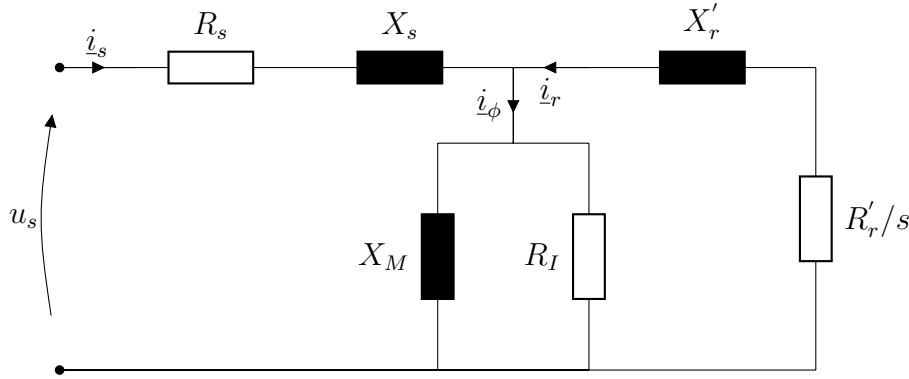

Figure 2.2: Equivalent circuit of and induction machine according to IEEE standard.

Where:
- R_s: Stator Resistance.
- X_s: Stator Leakage Inductance.
- X_M: Magnetizing Inductance.
- R_I: Iron Losses.
- R_r': Rotor Resistance referred to the stator.
- X_r': Rotor Leakage Inductance referred to the stator.
- u_s: Phase voltage.
- i_s: Current through one stator phase.
- i_r: Current through the rotor.
- i_ϕ: Current representing the magnetizing branch and iron losses.

This represents one phase of the motor, where at the left part represents the stator and at the right part the rotor. In between, two parallel branches appear, magnetizing or mutual, reactance and an iron loss representation can be found.

2.1.5 Losses

On an induction machine different kind of losses appear divided into.

1. Mechanical losses
   These appear because of all the frictional parts of the machine. They are concentrated to the bearings of the rotor.

2. Copper losses in the stator
   When the current goes through the windings conductors, unavoidable losses appear because of the Joule Effect. These can be described as

$$P_{Cu1} = 3R_s I_s \tag{2.2}$$

3. Core losses on the stator
   When current flows through the stator conductors, Eddy currents and Hysteresis losses appear in the iron laminations.

4. Copper losses on rotor
   It is the same as the copper losses due to Joule effect but as a result of the current going through the rotor. They can be described as

$$P_{Cu2} = 3R_r^{'}I_r^{'} \qquad (2.3)$$

5. Core losses in the rotor
   Losses due to the magnetic field are approximately proportional to the square of the frequency. As the rotor frequency is always lower than stator's, the iron losses in the rotor are usually neglected.

6. Stray load losses
   This clusters all the other electrical losses except for the one mentioned in items 2, 3, 4 and 5.

2.1.5.1 Skin Effect

Furthermore, an additional phenomenon can appear while the machine is working. Skin effect is not a loss by itself, but affects to electric drivers by modifying its resistance. When an AC current is going through a conductor, it has the tendency to be distributed in a way that the current density focuses near the external surface. Therefore, the effective section of the conductor narrows and the resistance is increased. This phenomenon becomes higher when the frequency is increased. When the conductors are small, this effect is negligible, as for the stator wires. However, because of the characteristics of a squirrel cage rotor, bars are bigger and has to be taken into account for high frequencies, usually over 50 Hz. One method to take this effect into consideration is to calculate the rotor parameters as a multiple-cage rotor model. [2]

3
Methods

In this chapter, the measurements and procedures that have been done are described. The main objective, as explained, was to test machine B and create two different models for each machine in two different software. Research is to be done respecting copyrights and legality, according to an ethical responsibility with environment. A list of all instrumentation used during the tests can be found next:

- Norma power meter: to calculate the rms values.
- 3 current sensors connected to the Norma power meter.
- Teledine LeCroy MDA805 oscilloscope: to record the waveforms.
- 3 Multimeters Fluke 175: for checking the voltage.
- Power supply Delta Elektronika SM 600-10

3.1   Machine B Measurements

As shown in Figure 2.2 the following parameters are necessary to describe the machine performance.

1. R_s: Stator Resistance
2. X_s: Stator Leakage Inductance
3. X_M: Magnetising Inductance
4. R_I: Iron Losses
5. $R_r^{'}$: Rotor Resistance
6. $X_r^{'}$: Rotor Leakage Inductance

As this machine was built to work in a wide range of frequencies, voltages and currents, it was important to obtain the values for different scenarios. For this reason, it is necessary to obtain them for a range of voltages, frequencies and currents. Blocked rotor test, no load test and disconnection test are used in order to determine all electric parameters.

3.1.1   Stator Resistance

In order to obtain the stator resistance, a direct current was fed between two of the lines with the power supply Delta Eletktronika. Measurements of the voltage were done for the 3 possible line combinations with the multimeters. With all the possibilities an average stator resistance could be obtained. Furthermore, it was possible to see if the resistance was current dependant. An end wye connection is

assumed and stator resistance for equivalent circuit is calculated as follows,

$$R_s = \frac{R_{DC}}{2} \tag{3.1}$$

where

R_s: Value of one line stator resistance [Ω]

R_{DC}: Value of resistance measured [Ω]

By performing a DC test to calculate the stator resistance, the skin effect cannot be taken into account. But actually, as the wires of the windings are made of small cross section strands, its effect is minor.

3.1.2 Blocked Rotor Test

Rotor and stator impedance can be calculated through a blocked-rotor test, which means that the shaft rotation is blocked trhough a mechanical device. With this restriction, the magnetizing resistance is high and the current through the rotor is higher than through the magnetizing branch. For this, the current through the magnetizing branch can be neglected. Then, for different levels of voltage and frequency, the blocked rotor leakage inductance, L_{BR}, and resistance, R_{BR} can be obtained. Taking these simplifications into account, the equivalent circuit for the test is as the shown in figure 3.1.
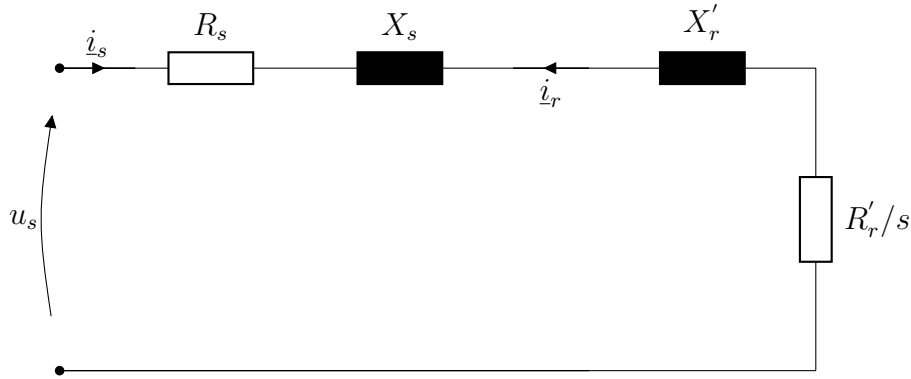

Figure 3.1: Equivalent circuit model for blocked-rotor test.

Whilst performing the tests, harmonics appeared in voltage. In order to force a more sinusoidal current wave, three resistors were added in series between the power supply and the machine. The resistors, shown in Figure 3.5, had a resistance value of 0,022 Ω, much higher than the stator resistance. The situation got better, but harmonics still appeared on the voltage for unknown reasons.

The setup established for doing the tests was as shown in Figures 3.2 and 3.3. The machine is connected to the voltage source (a large synchronous generator controlled with its control panel shown in Figure 3.4) with the 3-phase system and in series with each line with the resistor commented above. Two switches controlled the generator, control are to isolate the generator, and one more mechanical switch is located close to the machine. For security reasons a fuse of 200 A is also used.

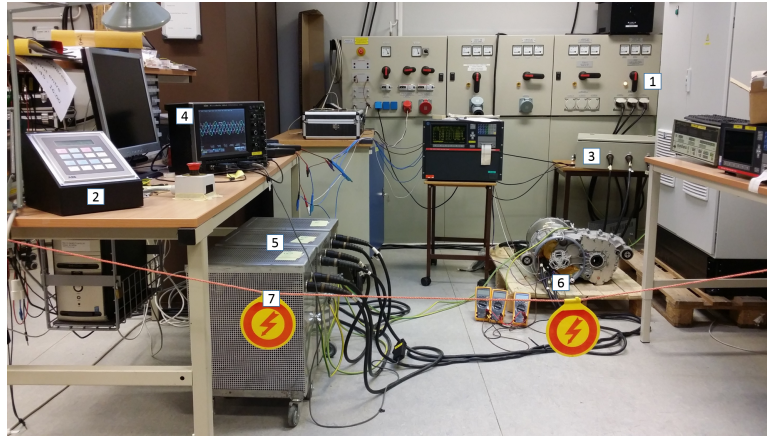**Figure 3.2:** Test setup for measurements. (1) Mechanical switch (2) Generator control panel (3) Current sensors (4) LeCroy Oscilloscope (5) Resistors (6) Machine (7) Security rope.

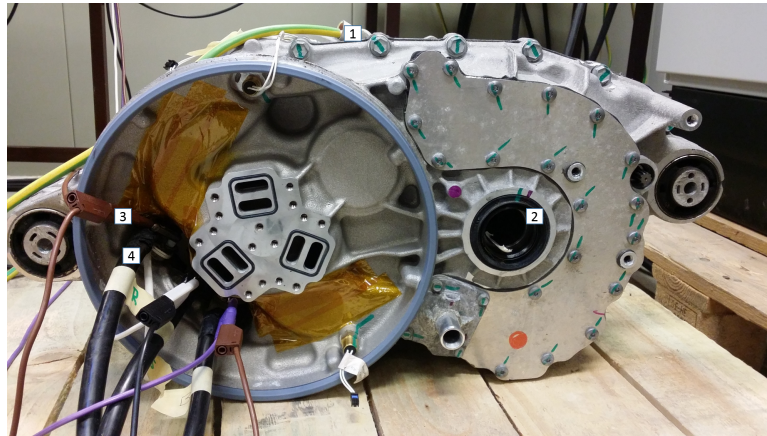**Figure 3.3:** Connection detail of the machine. (1) Ground connection (2) Output shaft gearbox (3) Voltage sensor connection (4) Grid connection.
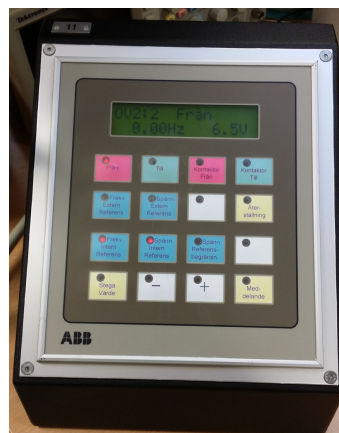
Figure 3.4: Control panel of the generator to select the voltage and the frequency supplied.

Figure 3.5: Resistors used for the tests connected on series between generator and machine.

The voltage was calculated by connecting the three phases directly of the oscilloscope to the closest point available of the stator whilst the neutral was simulated with a high impedance. A Norma powermeter was used to create this point by connecting the common point of voltage phases to the powermeter neutral. In order to block the rotation of the rotor, the gearbox available on the motor was used to add a resistance torque.

As the signal still had harmonics, as shown in Figure 3.6, using a power meter to obtain RMS or fundamental values worked badly. In order to proceed, the waveforms were recorded using a Lecroy oscilloscope and the waveforms were then analyzed with FFT. Afterwards, calculations were done with fundamental values.
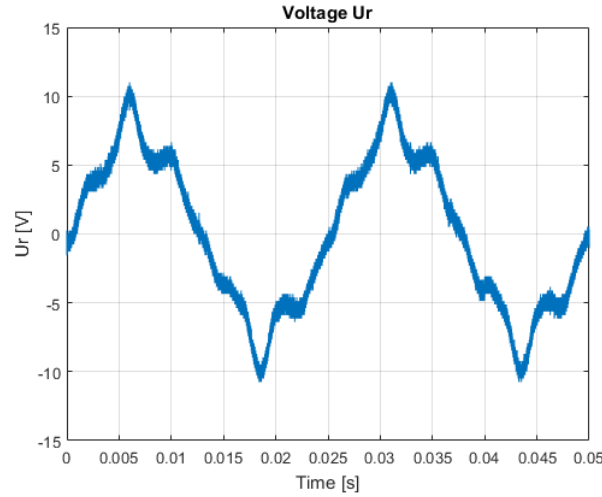
Figure 3.6: Graph of the voltage on machine side with resistors connected for 50 Hz and 4 V phase-neutral voltage.

In order to calculate the different parameters for the machine characterization, $I1_{BL}$, $V1_{BL}$ and P_{BL} were determined and the impedance parameters were determined using the relations

$$R_{BL} = \frac{P_{BL}}{3I1_{BL}^2} \qquad (3.2)$$

$$Z_{BL} = \frac{V1_{BL}}{I1_{BL}} \qquad (3.3)$$

$$X_{BL} = \sqrt{Z_{BL}^2 - R_{BL}^2} \qquad (3.4)$$

$$L_{BL} = \frac{X_{BL}}{2\pi f} \qquad (3.5)$$

where
R_{BL}: Value of resistance measured under blocked rotor conditions $[\Omega]$
P_{BL}: Power consumption by the motor at blocked rotor test $[W]$
I_1: Value of current for one line at blocked rotor test $[A]$
Z_{BL}: Impedance of the circuit machine under blocked rotor conditions $[\Omega]$
X_{BL}: Reactance measured at blocked rotor circuit $[\Omega]$
L_{BL}: Inductance of blocked rotor test circuit $[H]$
f: Frequency of the voltage supplied $[Hz]$
$V1_{BL}$: Voltage measured between phase-neutral $[V]$

Making the assumption that $X_r + X_M \gg R_r$, R_r should be calculated as follows

$$R_r = (\frac{X_s + X_M}{X_M})^2 \cdot (R_{BL} - R_s) \qquad (3.6)$$

where
R_r: Rotor resistance $[\Omega]$

X_s: Stator reactance $[\Omega]$
X_M: Magnetising reactance $[\Omega]$
R_{BL}: Value of resistance measured under blocked rotor conditions $[\Omega]$
R_s: Stator resistance $[\Omega]$

However, the problem was that the value of R_r was very low and could not be calculated in this way, and an alternative was presented in section 3.1.4.

3.1.3 No Load Test

In order to obtain X_1, R_I and X_M a test without load on the shaft was carried out on the motor. As before, to be able to determine all parameters under all case scenarios, different ratios of voltage and frequency were applied. When a no load test is developed, the slip of the induction machine is very small, assumed as 0, hence the resistive path of the rotor is very high and the current through it can be neglected. The resulting scheme is presented in Figure 3.7.
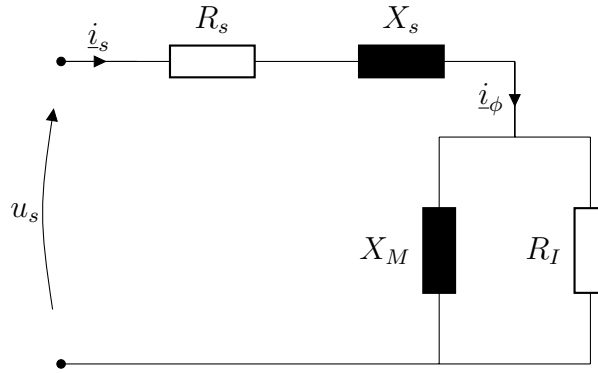
Figure 3.7: No load scheme circuit.

The setup was the same as the one used for the blocked rotor. The assumption of no load, even with the gearbox connected, was made as a dismantling was troublesome.

The measurements were recorded with the oscilloscope and processed using Matlab as well. V_0, P_0 and I_0 were directly obtained and from these equations parameters are determined. The impedance Z_0 can be found as

$$Z_0 = \frac{V_0}{I_0} \tag{3.7}$$

where V_0 is the phase voltage for no load conditions and I_0 is the current through one line for no load conditions.
The resistance of the no load model can be found as

$$R_0 = \frac{P_0}{3I_0^2} \tag{3.8}$$

where P_0 is the total power consumption for no load conditions.

And finally, the impedance of the equivalent no load circuit X_0 can be found as

$$X_0 = \sqrt{Z_0^2 - R_0^2} \tag{3.9}$$

By operating the motor under no load conditions, the powers can be obtained. P_0 is the no load power consumption and can be separated as

$$P_0 = P_{rot} + P_{Cu} \tag{3.10}$$

where P_{rot} is the power of rotational losses and P_{Cu} the total power losses of the cooper.
These later are calculated according to

$$P_{Cu} = 3R_s I^2 \tag{3.11}$$

Moreover, rotational losses can be detached into the losses due to the mechanical movement and the iron losses as follows

$$P_{rot} = P_{FE} + P_{Mec} \tag{3.12}$$

3.1.4   Rotor Resistance

The measurement of the rotor resistance through the blocked rotor resistance was really bad, and in some cases the value was nearly 0 Ω. As known, when a disconnection is produced on a motor, the machine keeps moving while breaking. The flux inside does not disappear immediately and the voltage decays according to the open-circuit time constant. For this, starting with a no load test, a disconnection of the power supply was done whilst the voltage was being measured. Afterwards, the time decay of the voltage was calculated as shown below, [4] [5] [6]

$$U_s = C\, w_{rr} \, \exp(-\frac{t}{\tau_r}) \tag{3.13}$$

where
$\quad U_s$: Voltage $[V]$
$\quad C$: A constant value $[\,]$
$\quad w_{rr}$: Wave part of the signal $[rad/s]$
$\quad \tau_r$: Time decay $[H/\Omega]$

and,

$$\tau_r = \frac{L_o}{R_r} \tag{3.14}$$

where
$\quad \tau_r$: Time decay $[H/\Omega]$
$\quad L_o$: Rotor leakage inductance $[H]$
$\quad R_r$: Resistance of the rotor $[\Omega]$

Assuming that $X_0 = X_s + X_M$,

$$X_s = \frac{X_{BL}}{2} \tag{3.15}$$

$$L_s = \frac{X_s}{2\pi f} \tag{3.16}$$

and then $L_s = L_r$. With this, L_r is calculated and consequently R_r with (3.14).

3.1.5 Determination of Inertia

It is necessary to determine the inertia of the machine for obtaining a transient model of the machine. For this, a method is applied where the machine is energized to a no-load operation point and then it is disconnected from the grid and allowed to continue to rotate. During this period the voltage decay and current is measured. The equation that determines the inertia is as follows,

$$J\frac{d\omega}{dt} = T_e - T_m \tag{3.17}$$

where
   J: Mechanical inertia of the machine $[Kgm^2]$
   $d\omega/dt$: Differential temporal variety of angular speed $[rad/s]$
   T_e: Electromagnetic torque $[Nm]$
   T_m: Mechanical Torque on the shaft $[Nm]$

The ratio $\frac{d\omega}{dt}$ can be calculated by measuring the variation of the frequency along the time whilst the machine is slowing down, immediately after the disconnection. The torque on the shaft is calculated at the previous instant before the disconnection with the power and the speed

$$T_m = \frac{P_{NL}}{\omega} \tag{3.18}$$

where
   P_{NL}: Power from the no load test $[W]$
   T_m: Mechanical torque on the shaft $[Nm]$
   ω: Mechanical speed of the shaft $[rad/s]$

From (3.17) two different things can be observed. Firstly, when the machine is rotating, the left part of the equation is 0, therefore the electromagnetic torque is equal to the mechanical shaft torque, and T_e can be calculated with ease without the necessity of knowing the rotor current. Even though, at the moment of the disconnection, the stator current drops rapidly to zero, therefore the copper losses must be removed from the no load power and a percentage of the iron losses as well, and it is calculated as

$$P_e = P_{NL} - P_{Cu} - 0,1 P_{FE} \tag{3.19}$$

and

14

$$T_e = \frac{P_e}{\omega} \tag{3.20}$$

Secondly, from the moment of the disconnection until the stator's voltage is zero, the magnetic flux generated is zero and consequently also the electromagnetic torque, thus making the calculation of J along disconnection time possible.

In order to calculate the decrease of the frequency over time, a PLL was used. The PLL was set to follow the voltage and determine the value of the frequency for the retardation process.

3.2 Machine A Modelling

3.2.1 MotorCAD Design

First of all, a model of the machine was set up. Data of this machine was known and results of the model could be compared in order to validate it. The machine was a 15 kW from ABB with model number MBT 180L. The configuration of the model for the 15 kW machine is shown in Figure 3.1 and 3.2.

3.2.1.1 Geometry Configuration

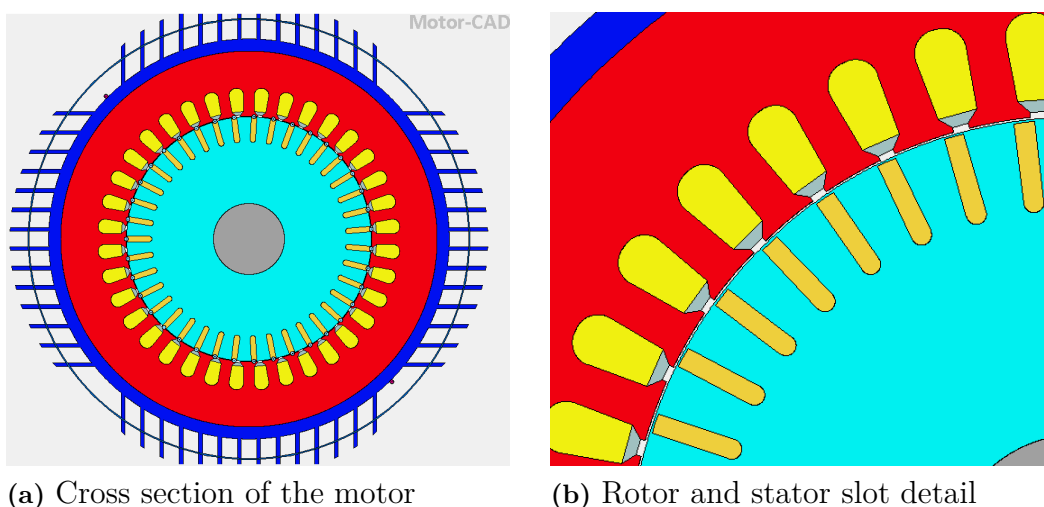The values used for stator and rotor dimensions are shown below.

(a) Cross section of the motor   (b) Rotor and stator slot detail

Figure 3.8: Motor A geometry in MotorCAD.

Table 3.1: Geometry parameter values of rotor and stator for machine A.

Stator Data		Rotor Data	
Parameter	Value	Parameter	Value
Slot Number	36	Rotor Bars	39
Housing Dia	310	Bar Opening [T]	0
Stator Lam Dia	291,2	Bar Opening Depth [T]	0,5
Stator Bore	190,2	Bar Tip Angle [T]	0
Slot Width (Bottom)	11	Bar Depth [T]	17
Slot Width (Top)	8,5	Bar Width [T]	4,3
Slot Depth	22	Bar Opening [B]	4,3
Slot Corner Radius	5	Bar Opening Depth [B]	0
Tooth Tip Depth	1	Bar Width [B]	4,3
Slot Opening	3,5	Airgap	0,45
Tooth Tip Angle	45	Banding Thickness	0
Sleeve Thickness	0	Shaft Dia	55
Fin Extension	30	Shaft Hole Diameter	0
Fin Thickness	3		
Fin Number [Quadrant]	14		
Fin Spacing [Fin Base]	12		
Corner Cutout [%]	36,129		
Cowling Thickness	1		
Cowling Radial Gap	-15		

Apart from rotor and stator dimensions, other values, as bearings and cage dimensions, were necessary. While the values of the parameters that have been set do not match with the real geometry, this has been done because of the lack of resources to define them through the software. As for example, for the slots, a few geometry parameters can be set and even the shape possibilities are different to the one desired. It has to be assured that model works and still represents the real machine.
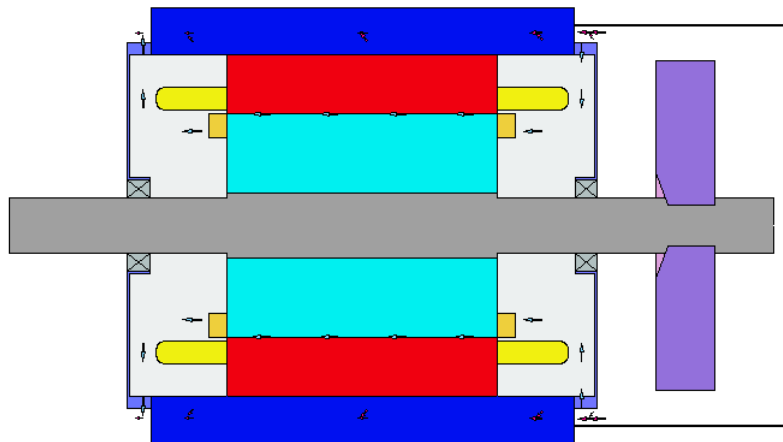

Figure 3.9: Axial geometry of motor A.

Table 3.2: Radial and axial general data for machine A.

Radial General Data		Axial General Data	
Parameter	Value	Parameter	Value
Housing Dia	360 mm	Motor Length	400 mm
Housing Add [Outer F]	0 mm	Stator Lam Length	230 mm
Housing Add [Outer R]	0 mm	Rotor Lam Length	230 mm
Stator Lam Dia	291,2 mm	Stator Axial Offset	0 mm
Stator Bore	190,2 mm	Rotor Axial Offset	0 mm
Airgap	0,45 mm	Ewdf Overhang [F]	60 mm
Banding Thickness	0 mm	Ewdf Overhang [R]	60 mm
Sleeve Thickness	0 mm	Wdg Extension [F]	0 mm
EndRing Add [Outer F]	0 mm	Wdg Extension [R]	0 mm
EndRing Add [Inner F]	0 mm	Endcap Length [F]	20 mm
EndRing Add [Outer R]	0 mm	Endcap Length [R]	20 mm
EndRing Add [Inner R]	0 mm	Endcap Thickness [F]	2 mm
Wafter Number [F]	0 mm	Endcap Thickness [R]	2 mm
Wafter Number [R]	0 mm	EndRing Thickness [F]	15 mm
Shaft Dia	55 mm	EndRing Thickness [R]	15 mm
Shaft Dia [F]	48 mm	EndRing Extension [F]	0 mm
Shaft Dia [R]	48 mm	EndRing Extension [R]	0 mm
Shaft Hole Diameter	0 mm	Shaft Extension [F]	100 mm
Wdg Add [Outer F]	0 mm	Shaft Extension [R]	150 mm
Wdg Add [Outer R]	0 mm	Bearing Width [F]	19 mm
Wdg Add [Inner F]	0 mm	Bearing Width [R]	19 mm
Wdg Add [Inner R]	0 mm	Bearing Offset [F]	0 mm
EWdg Insulation [F]	0 mm	Bearing Offset [R]	0 mm
EWdg Insulation [R]	0 mm	Stator Plate Thick [F]	0 mm
Bearing Dia [F]	77,5 mm	Stator Plate Thick [R]	0 mm
Bearing Dia [R]	77,5 mm	Cowling Length	185 mm
Fin Extension	30 mm	Cowling Axial Gap	165 mm
Cowling Thickness	1 mm	Fan Axial Position	450 mm
Cowling Radial Gap	-15 mm	Fan Blade Width	50 mm
Fan Blades	8 mm	Fan Blade Offset	0 mm
Fan Blade Thickness	2 mm	Fan Backplate Width	10 mm
Fan Diameter	280 mm	Fan Hub Extension	0 mm
Fan Backplate Dia	90 mm		
Fan Hub Dia	35 mm		

3.2.1.2 Winding Pattern

In this motor, 2 strands make up each conductor. The machine winding is divided into 3 parallel paths. The number of turns was 38, and the pattern was AABBCC, as can be seen from figure 3.10. The windings are star connected.
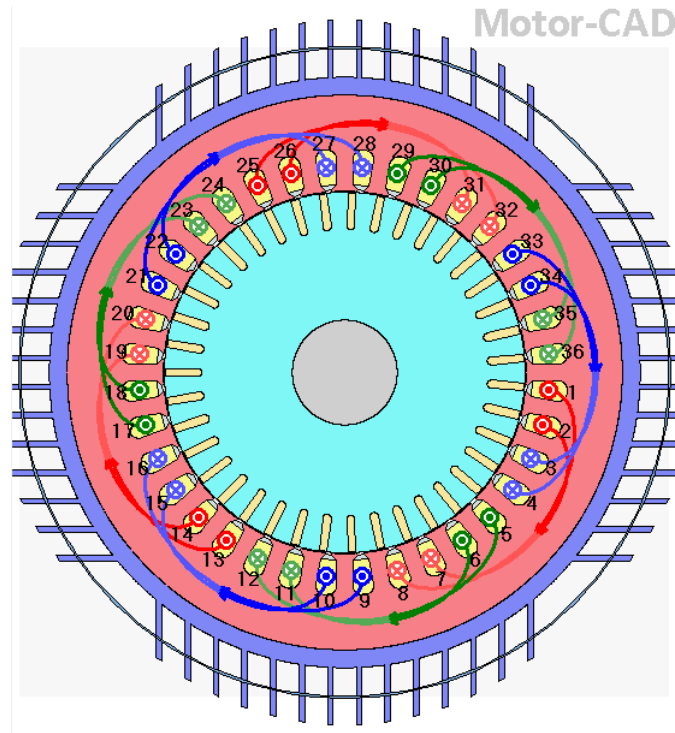
Figure 3.10: Winding pattern for machine A.

The diameter of the wire was set to 1,18 mm with a copper diameter of 1,08 mm. Therefore, the area of the stator slot was 191,8 mm^2 with an area of 168 mm^2 for the windings. Whilst the copper area was 69,62 mm^2, leading to a copper slot fill of 36,3%.

For setting the pattern, a script calculation with dimensional parameters was set in order to calculate the stator resistance previously and validate that the model would match. The different parameters are calculated as follows

$$Span\_per\_winding = \frac{Perimeter}{Poles} \tag{3.21}$$

and

$$End\_winding\_length = Output\_extension + f_k \cdot Span\_per\_winding \tag{3.22}$$

where f_k is an empirical factor set to 1,2.

The different values used for the pattern selected are presented in Table 3.3.

Table 3.3: Parameters to validate winding pattern through 1 phase stator resistance for machine A.

Parameter	Value
Slots per phase pole	2
Turns per coil	38
Stator active length	230 mm
Number of poles	6
Diameter of slot stator center	215 mm
Perimeter	675 mm
Span per winding	113 mm
End winding length	195 mm
Wire length	425 mm
Resistivity of the conductor	1,68E-8 Ω m
Wire diameter	1,08 mm
Resistance of 1 strand	1,1849 Ω
Number of strands	2
Resistance of strands	0,5925 Ω
Number of parallel branches	3
Stator Resistance	0,1975 Ω

3.2.1.3 Materials

Different materials were set for the components of the motor. Both stator and rotor laminations were made of steel M700-50A. The wires of the stator windings were made of copper and the rotor cage was made of aluminium. Magnetization data for M700-50A was only available until 1,8 T, but a higher point of 1,5 MA/m at 3,8 T was set up in order to force the B-H curve to be realistic. This data can be found in Appendix A.1.1, A.1.

3.2.2 Maxwell Design Machine A

Experiments were performed on machine A previously and the data is available for reference [2] [3]. A basic model of machine A in Ansys Maxwell is built referring to the methodologies explained in Ansys Maxwell manual for PRIUS motor model and induction machine.

3.2.2.1 Present Data

For machine A, geometrical and measured data are available from previous measurements [2][3]. Material of stator and rotor material is taken as described in section 3.2.1.3. Stator and rotor data are presented in tables 3.4. Similarly the stator and rotor slots are designed as per table 3.9.

The air gap, defined as the gap between stator and rotor of a machine was found to be 0,45 mm in the same article. The present analysis of machine A in Maxwell is carried out at 20°C and the air gap is maintained accordingly by taking suitable value of rotor outer diameter as mentioned in table 3.9. Since the tooth tip angle is
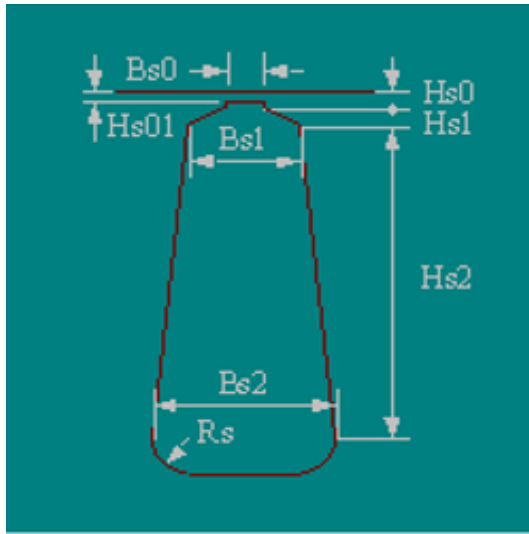
not known and the slot is visible but not accessible for measurement in machine A, it is assumed to be 45° and hence the parameter 'Hs1' is set to 3 (refer to fig.3.9) and Maxwell output is presented in fig.3.14. Visual observation and Maxwell model confirms the value of tooth tip angle to be same i.e. 45°. Machine A wire diameter is measured with a gauge meter and found around 1,18 mm.
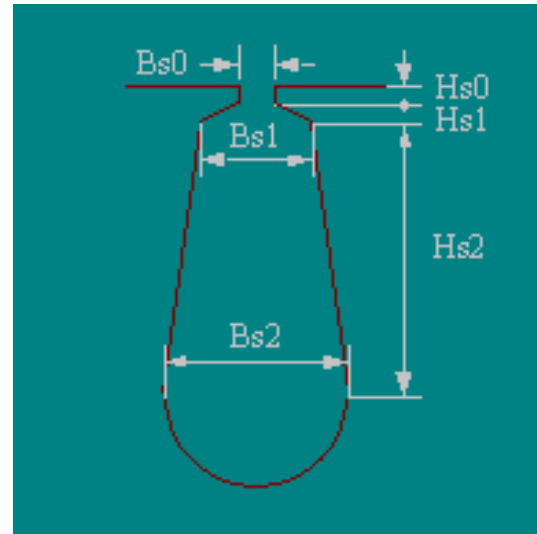
Table 3.4: Stator and rotor dimension

Rotor Data	
Parameter	Value
Outer Diameter	189,3 mm
Inner Diameter	55 mm
Length	230 mm
Stacking factor	0,95
Steel Type	M700-50A
Number of slots	39
Slot Type	3

Stator Data	
Parameter	Value
Outer Diameter	291,2mm
Inner Diameter	190,2mm
Length	230 mm
Stacking factor	0,95
Steel Type	M700-50A
Number of slots	36
Slot Type	2

Table 3.5: Stator and rotor slot data

Rotor Slot Data	
Parameter	Value in mm
Hs0	0,5
Hs01	0,5
Hs1	0,2
Hs2	12
Bs0	3,4
Bs1	3,5
Bs2	3,9
Rs	1

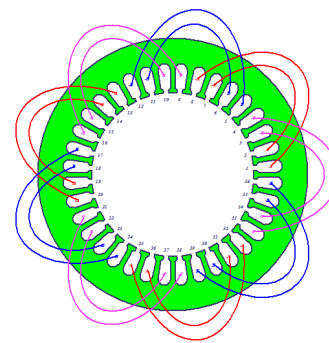| Stator Slot Data	
Parameter	Value in mm
Hs0	1
Hs1	3
Hs2	20,85
Bs0	3,5
Bs1	8,5
Bs2	11

(a) Rotor slot

(b) Stator slot

Figure 3.11: Machine A stator slot and rotor slot

Figure 3.12: Measurement of wire width

	Phase	Turns	In Slot	Out Slot
Coil_1	A	76	1	8
Coil_2	A	76	2	7
Coil_3	-C	76	3	34
Coil_4	-C	76	4	33
Coil_5	B	76	5	12
Coil_6	B	76	6	11

(a) Stator coil connection table

(b) Stator winding arrangement

Figure 3.13: Machine A stator winding connection arrangement
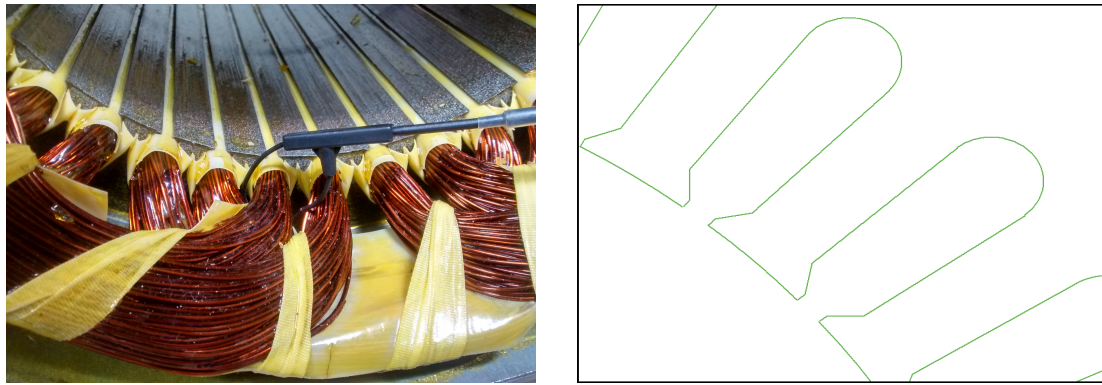
(a) Winding arrangement of 15 kW IM   **(b)** Stator slot angle
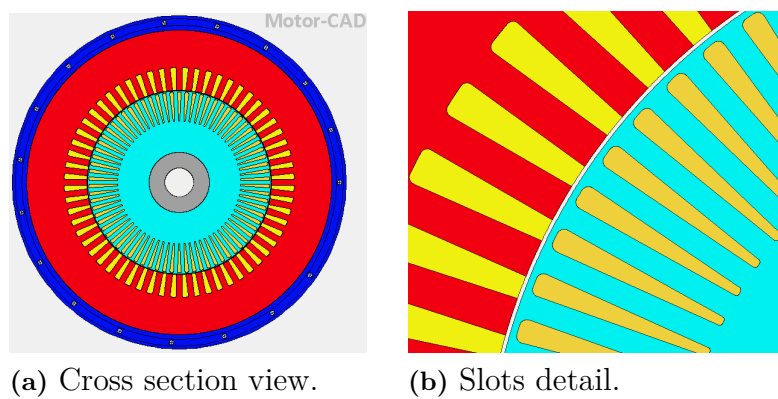
Figure 3.14: Stator winding arrangement in IM

3.3 Machine B Modelling

3.3.1 MotorCAD Design

3.3.1.1 Geometry Configuration

The values used for stator and rotor dimensions were measured from the machine and are presented in Table 3.6 and represented in Figure 3.15.

(a) Cross section view.   **(b)** Slots detail.

Figure 3.15: Machine B geometry in MotorCAD.

Table 3.6: Geometry parameter values of rotor and stator for machine B.

Stator Data		Rotor Data	
Parameter	Value	Parameter	Value
Slot Number	60	Rotor Bars	74
Housing Dia	277	Pole Number	4
Stator Lam Dia	253	Bar Opening [T]	0
Stator Bore	157	Bar Opening Depth [T]	0,87
Tooth Width	5	Bar Opening Radius [T]	0,93
Slot Depth	19	Rotor Tooth Width [T]	3,2
Slot Corner Radius	0	Bar Depth [T]	24,2
Tooth Tip Depth	0	Bar Corner Radius [T]	0,418
Slot Opening	3,22027	Airgap	0,6
Tooth Tip Angle	0	Banding Thickness	0
Sleeve Thickness	0	Shaft Dia	50
WJ Channel-Lam	3,9	Shaft Hole Diameter	24
WJ Channel Height	5,6		

Apart from rotor and stator dimensions, other values, as bearings and cage dimensions had to be approximately assumed. These are presented in Table 3.7 and a scheme is shown in Figure 3.16.
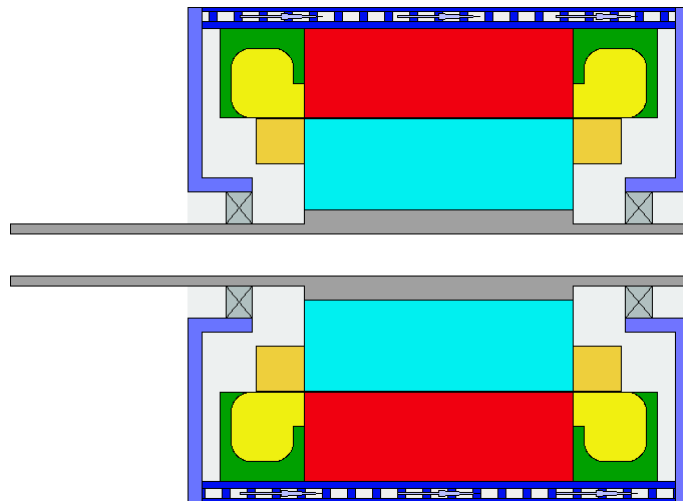

Figure 3.16: Axial geometry view of machine B in MotorCAD.

Table 3.7: Radial and axial general data for machine B.

Radial General Data		Axial General Data	
Parameter	Value	Parameter	Value
Housing Dia	277 mm	Motor Length	280 mm
Housing Add [Outer F]	0 mm	Stator Lam Length	150 mm
Housing Add [Outer R]	0 mm	Rotor Lam Length	150 mm
Stator Lam Dia	253 mm	Stator Axial Offset	0 mm
Stator Bore	157 mm	Rotor Axial Offset	0 mm
Airgap	0,60 mm	Ewdg Overhang [F]	41 mm
Banding Thickness	0 mm	Ewdg Overhang [R]	41 mm
Sleeve Thickness	0 mm	Wdg Extension [F]	6 mm
EndRing Add [Outer F]	0 mm	Wdg Extension [R]	6 mm
EndRing Add [Inner F]	0 mm	Endcap Length [F]	8 mm
EndRing Add [Outer R]	0 mm	Endcap Length [R]	8 mm
EndRing Add [Inner R]	0 mm	Endcap Thickness [F]	8 mm
Wafter Number [F]	0 mm	Endcap Thickness [R]	8 mm
Wafter Number [R]	0 mm	EndRing Thickness [F]	27 mm
Shaft Dia	50 mm	EndRing Thickness [R]	27 mm
Shaft Dia [F]	35 mm	EndRing Extension [F]	0 mm
Shaft Dia [R]	35 mm	EndRing Extension [R]	0 mm
Shaft Hole Diameter	24 mm	Shaft Extension [F]	120 mm
Wdg Add [Outer F]	20 mm	Shaft Extension [R]	21 mm
Wdg Add [Outer R]	20 mm	Bearing Width [F]	15 mm
Wdg Add [Inner F]	0 mm	Bearing Width [R]	15 mm
Wdg Add [Inner R]	0 mm	Bearing Offset [F]	21 mm
EWdg Insulation [F]	0 mm	Bearing Offset [R]	21 mm
EWdg Insulation [R]	0 mm	Stator Plate Thick [F]	0 mm
Bearing Dia [F]	70 mm	Stator Plate Thick [R]	0 mm
Bearing Dia [R]	70 mm	WJ Channel Width	9,5 mm
WJ Channel-Lam	3,9 mm	WJ Channel Spacing	4,5 mm
WJ Channel-Height	5,6 mm	Potting-Endcap [F]	10 mm
Potting-Housing [F]	0 mm	Potting-Endcap [R]	10 mm
Potting-Housing [R]	0 mm		

3.3.1.2 Winding Pattern

Different possibilities of winding pattern were possible. It was known that through one stator slot 52 conductors were present and that it is a 3 phase machine. Moreover, it was assumed to be a 4 pole machine and wye connected. However, that was not enough and different patterns were possible. By doing measurements with a multimeter on half of the stator of the machine and with the calculation script presented in section 3.2.1.2, it was possible to find one feasible winding pattern in order to make it match with the stator resistance. As the wire diameter was an unknown value, a visual inspection was done and it was calculated to be 1,1 mm. However, when the cutting of the stator was done, it could have deformed the wires and these could seem bigger. This size is a critical parameter, as the stator resis-

tance is quite sensitive to it. Moreover, it was taken into account that the copper slot fill factor that could be obtained by changing this parameter had to be between 41% and 43%, and a study of the stator resistance sensitivity in function of the wire diameter was done and it is shown in Figure 3.17.
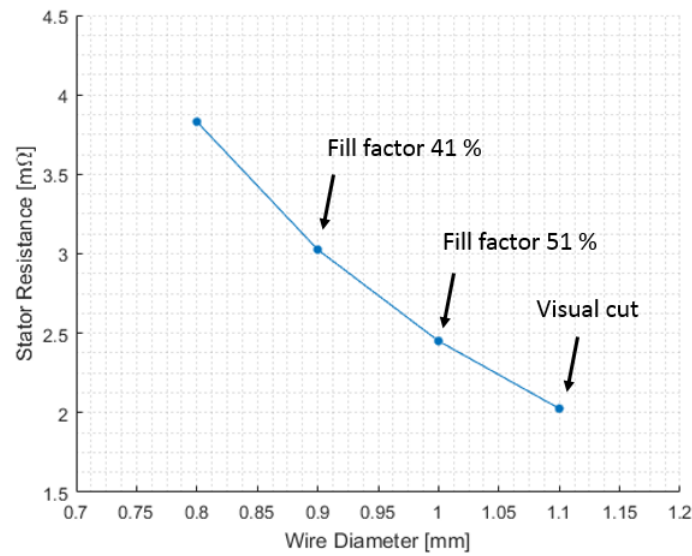

Figure 3.17: Values of the calculated stator resistance for different wire diameters for machine B.

Finally, a wire diameter of 0,9 mm was selected in order to obtain a proper copper slot fill factor and to obtain a calculated stator resistance that matched with the previous measurements done to machine B. The different values used for the pattern selected were calculated with (3.21) and (3.22) and are presented in Table 3.8.

Table 3.8: Parameters to validate winding pattern through stator resistance for machine B.

Parameter	Value
Slots per phase pole	5
Turns per coil	1
Number of winding layers	2
Stator active length	150 mm
Number of poles	4
Diameter of slot stator center	175 mm
Perimeter	550 mm
Span per winding	137 mm
End winding length	205 mm
Wire length	355 mm
Resistivity of the conductor	1,68E-8 Ω m
Wire diameter	0,9 mm
Resistance of 1 strand	0,1574 Ω
Number of strands	26
Resistance strands	0,0061 Ω
Number of parallel branches	2
Stator Resistance	0,003026 Ω

Therefore, a double layer pattern with upper and bottom slot configuration was set up. Every 5 slots there is always 2 different phases in a slot, as can be seen in Figure 3.18. It consists of 2 parallel branches per phase, doing 1 turn through 5 slots and then going in series to another 5 slots. Therefore, the winding has 2 different ending points, one for each parallel branch.
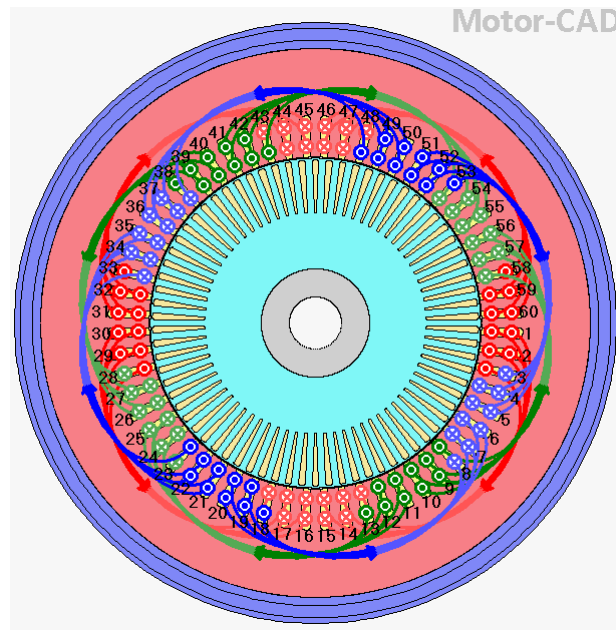
Figure 3.18: Winding pattern of machine B in MotorCAD.

3.3.1.3 Materials

Different materials were set for the components of the motor. The wires of the windings were copper and the rotor cage was set to copper. Both stator and rotor laminations were calculated with steel M235-50A having a resistivity of 5,9E-7 Ωm and magnetization data that can be found in A.1.2 with loss model as well. For the M235-35A magnetizing curve, only data until 1,8 T was available, therefore a higher point was set up to properly model saturation. All data can be found in section A.1.

3.3.2 Maxwell Design Machine B

As per the measurement of machine B stator slot area is 80,09 mm^2 and copper area is 36,86 mm^2 giving a slot fill factor of 46,02%.

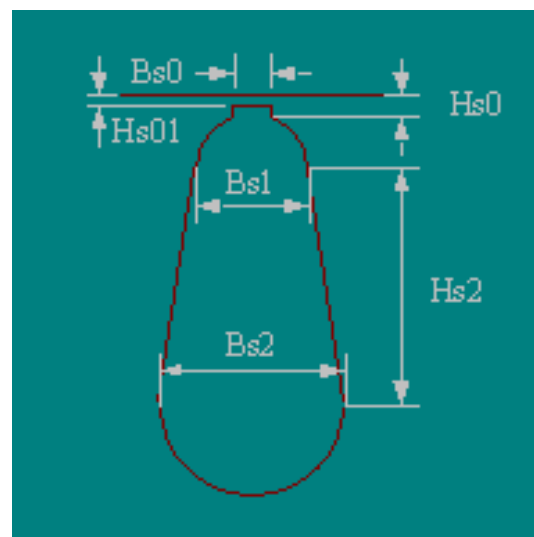**Table 3.9:** Stator and rotor slot data

Stator Slot Data	
Parameter	Value in mm
Hs0	0,15
Hs01	0
Hs1	0,5
Hs2	19
Bs0	3,22027
Bs1	2
Bs2	6
Rs	1

Rotor Slot Data	
Parameter	Value in mm
Hs0	0,87
Hs01	0,87
Hs1	0,93
Hs2	24,2
Bs0	0,001
Bs1	3,2
Bs2	0,93
Rs	0,5
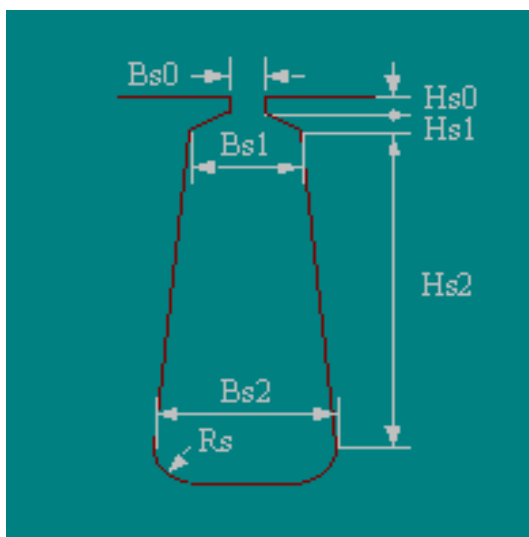
(a) Stator slot

(b) Rotor slot

Figure 3.19: Machine B stator slot and rotor slot in Maxwell

	Phase	Turns	In Slot	Out Slot
Coil_1	A	26	1T	15T
Coil_2	A	26	1B	15B
Coil_3	A	26	2T	14T
Coil_4	A	26	2B	14B
Coil_5	A	26	3B	13B
Coil_6	C	26	53T	3T
Coil_7	C	26	52T	4T
Coil_8	C	26	52B	4B
Coil_9	C	26	51T	5T
Coil_10	C	26	51B	5B
Coil_11	C	26	20T	6T
Coil_12	C	26	20B	6B
Coil_13	C	26	19T	7T
Coil_14	C	26	19B	7B
Coil_15	C	26	18T	8T
Coil_16	B	26	8B	58B
Coil_17	B	26	9T	57T
Coil_18	B	26	9B	57B
Coil_19	B	26	10T	56T
Coil_20	B	26	10B	56B

(a) Stator coil connection table
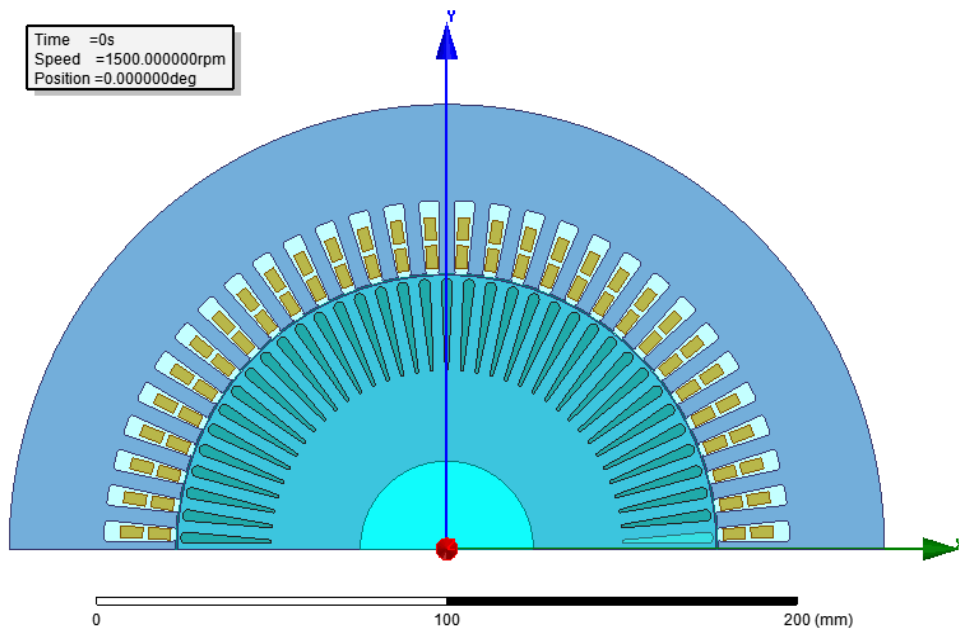
(b) Stator winding arrangement

Figure 3.20: Machine B stator winding connection arrangement in Maxwell

4

Analysis

4.1 Machine B Measurements

4.1.1 Stator Resistance

With the methodology followed as described in 3.1.1, the following values of voltage and currents were obtained and presented in Table 4.1.

Table 4.1: Values of measured voltages for DC testing at machine B.

Current (A)	Voltage AB (V)	Voltage AC (V)	Voltage BC (V)
1	0,006	0,006	0,006
2	0,011	0,011	0,011
5	0,029	0,028	0,028
10	0,057	0,057	0,056
12	0,072	0,068	0,071
15	0,088	0,086	0,086
20	0,115	0,113	0,114

Using a wye connection model, the average resistance was calculated accordingly to (3.1) and presented in Table 4.2.

Table 4.2: Values of average R_s for different currents.

Current (A)	Average R_s ($m\Omega$)
1	3,0
2	2,7
5	2,8
10	2,8
12	2,9
15	2,8
20	2,8

Consequently, the stator resistance was assumed to be 0,0028 Ω for the upcoming calculations.

4.1.2 Blocked Rotor Test

For the blocked rotor tests, the phase supply voltage and line current were recorded from the oscilloscope. As example, one case is shown in Figure 4.1.
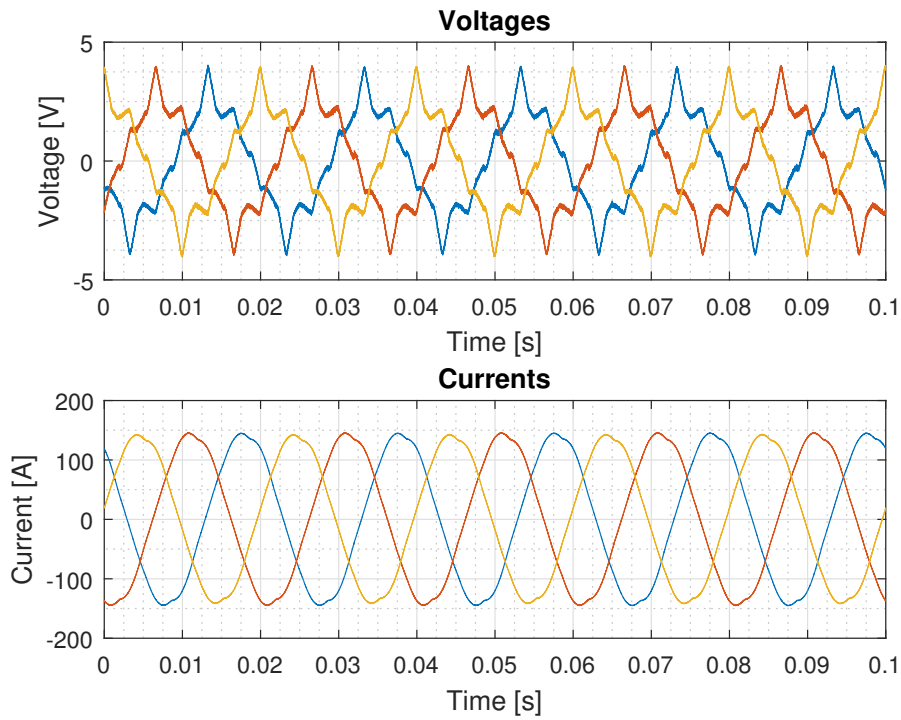

Figure 4.1: Voltage and current wave measurements of blocked rotor tests on machine B.

As can be seen, the voltage was not a very sinusoidal wave. The reason is the non-linearity of the investigated induction machine, mainly caused by the closed rotor slots. From the tests and procedure explained following results were obtained. A graph for R_{BL} is shown in Figure 4.2 and for L_{BL} in Figure 4.3 for different frequencies and current level. These are calculated from the fundamental values of the waves.
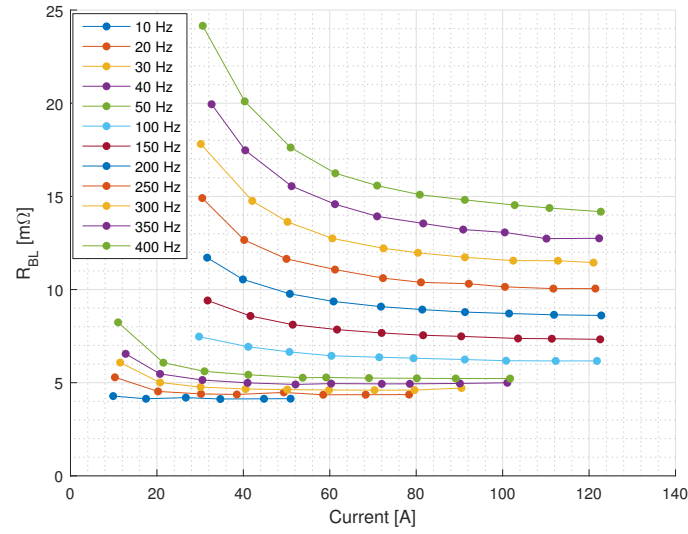
Figure 4.2: Resistance calculated from blocked rotor tests over current for machine B.
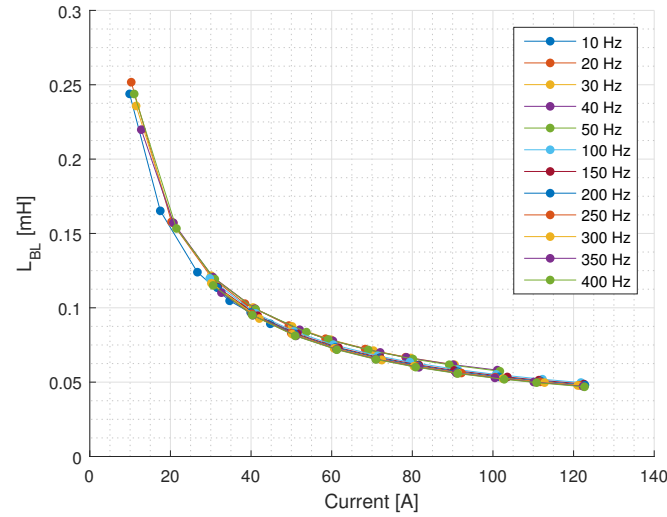

Figure 4.3: Inductance calculated from blocked rotor test for machine B.

L_{BL} is strongly current dependant and the shape is formed due to fact that the rotor bars are completely enclosed by the laminations. For low currents, the inductance is high but when current is high it acts as an open bar model. A graph of reactance over resistance for blocked rotor conditions is shown in Figure 4.4.
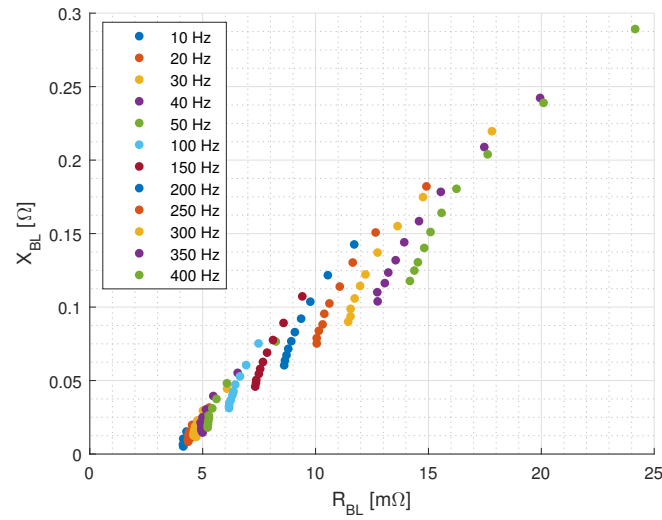
Figure 4.4: Impedance and resistance of blocked rotor test for machine B.

As can be seen, the results for the blocked rotor tests are as expected for an induction machine. And a normal performance is obtained from 10 Hz to 400 Hz and from 10 A to 120 A.

4.1.3 No Load Tests

For the no load tests, the phase supply voltage and current line are recorded using the oscilloscope. As an example, one case at 50 Hz and another at 350Hz are shown on Figure 4.5 and Figure 4.6.
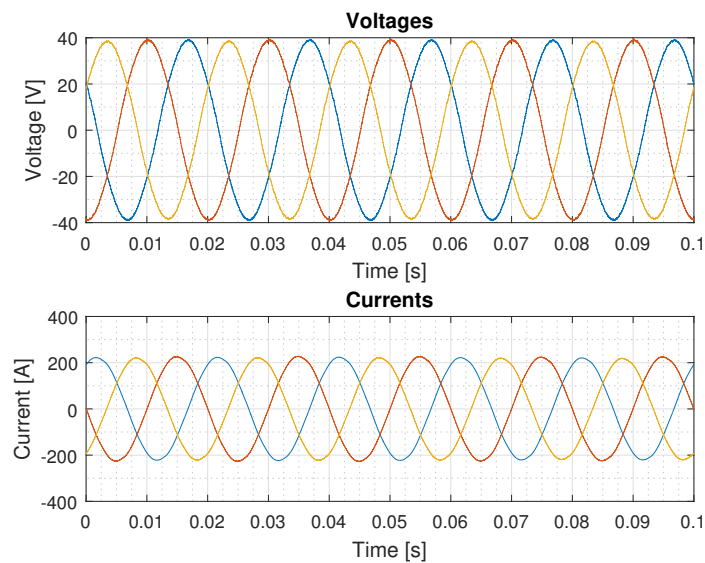

Figure 4.5: Voltages and currents waves of no load tests at 50 Hz.
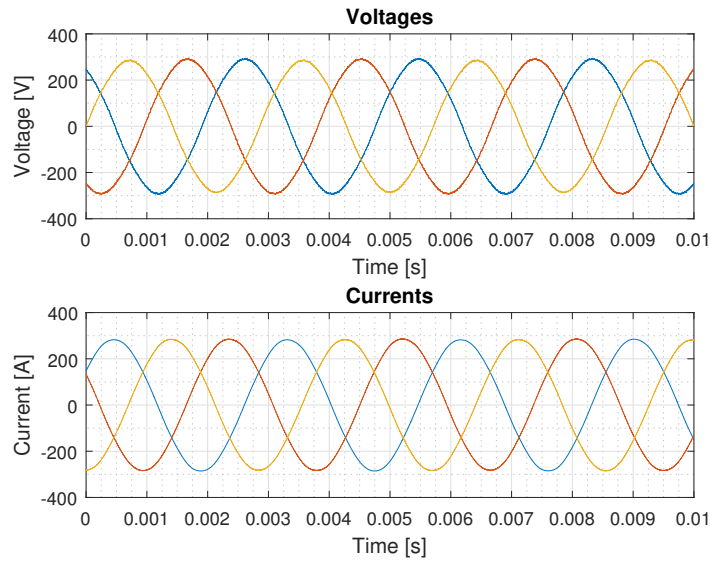
Figure 4.6: Voltages and currents waves of no load tests at 350 Hz.

Even at a peak of 280 V and 285 A no severe saturation effect is observed in the current waveform.

The results of the measurements are shown in graphs below. It is interesting to plot the value of L_o, in Figure 4.7, and the powers, in Figure 4.8, to understand the machine. All calculations are done with fundamental values after applying FFT.

Figure 4.7: Inductance calculated from no load tests at machine B.

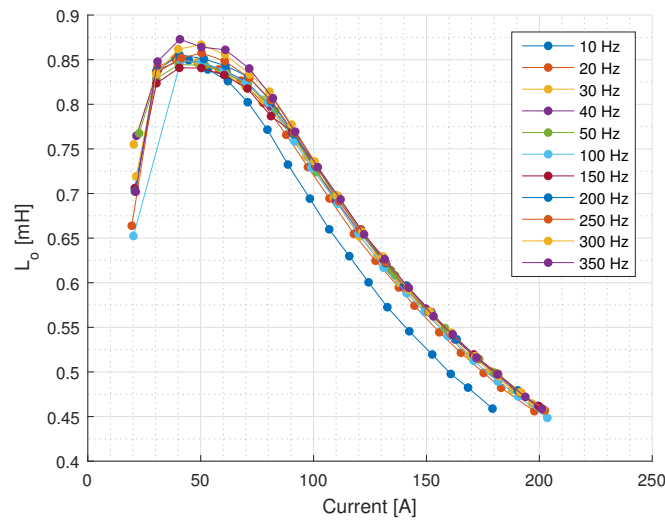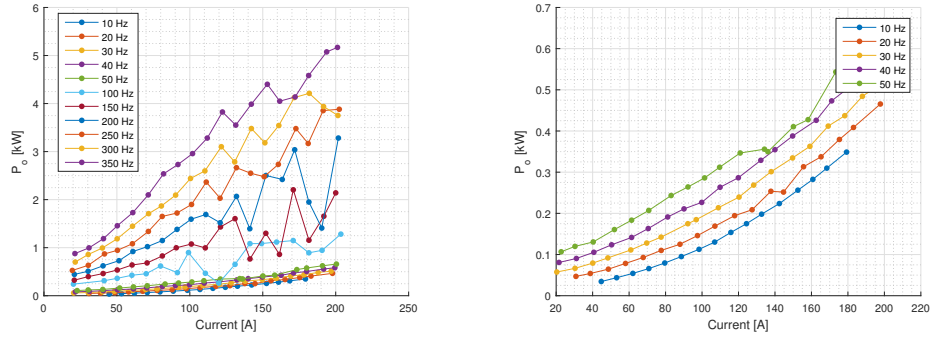**(a)** Power supplied for no load tests for machine B.

(b) Detail of the powers up to 50 Hz for machine B.

Figure 4.8: Power consumption of the machine B for no load conditions.

For the calculation of L_0, the results are clearly current dependant but independent of the frequency. Only the results from the 10 Hz case is slightly different for unknown reasons. Regarding the power measurement, it can be seen in Figure 4.8 that a clear tendency exists for low frequencies and for high frequencies until 80 A, but out of this region, the results are unstable and unpredictable. More tests were done to evaluate this situation, and they were not repeatable, accordingly these values were not used more.

In Figure 4.9 the rotational losses are presented. These are calculated as indicated in (3.10). Moreover, a detail of low frequencies, where the results more clearly follow a tendency, is shown.
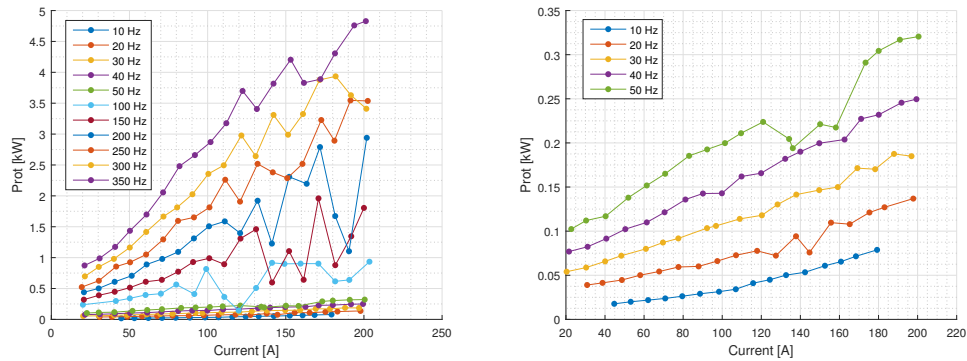
(a) Rotational losses of no load tests from machine B.

(b) Rotational losses of no load tests at low frequencies.

Figure 4.9: Rotational losses calculated from measurements for machine B.

As can be noticed, the tendency is only clear for frequencies lower than 100 Hz or for all frequencies under 80 A.

In figure 4.10, the rotational power losses are plotted over the square of voltage. The calculus with the square of the voltage helps to avoid error when the extrapolation

is done. From the point where the voltage is extrapolated to 0 V the mechanical friction losses can be identified. When the voltage is zero, there is no magnetic flux, therefore the iron losses are zero, and the calculation of iron losses is done by subtracting the mechanical losses from the rotational losses. A detail of low frequencies is shown as well.
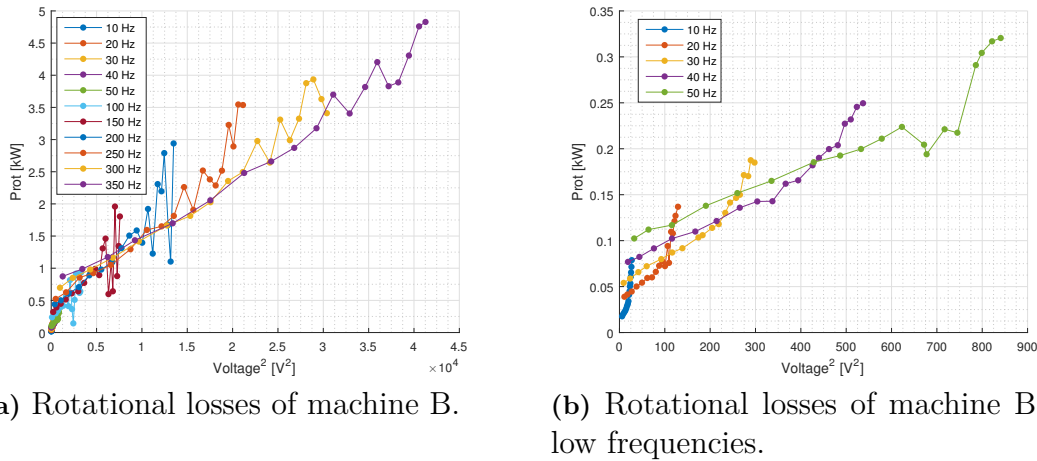

(a) Rotational losses of machine B.

(b) Rotational losses of machine B at low frequencies.

Figure 4.10: Rotational losses over square of voltage from measurements at no load conditions.

With the above information, the iron losses can be calculated for low frequencies. These are presented in Table 4.3.

Table 4.3: Values of rotational losses, iron losses and constant mechanical losses for machine B for different voltages and frequencies.

Freq (Hz)	Voltage (V)	Rot. Losses (W)	Iron Losses (W)	Mec. Losses (W)
10	5,21	78,8	68,5	10,5
20	11,36	136,9	102,4	34,5
30	17,26	185	133,7	51,3
40	23,18	249,6	175,7	73,9
50	28,00	320,5	228,3	92,2

As seen, the behaviour of power for frequencies higher than 50 Hz and over 100 A was unstable. By excluding these conditions, the results have a clear tendency. The response is as expected for an induction machine with a squirrel rotor cage. For high frequencies, the results cannot be neither accepted nor taken into consideration for simulations, as they are not consistent and also not repeatable for unknown reasons.

4.1.4 Rotor Resistance

As commented, the rotor resistance could not be calculated from the blocked rotor and no load test because a senseless value was obtained. However, with the following disconnection method it could be calculated. In Figure 4.11 it can be seen the voltage phase drop at 10 Hz and the line current as well.
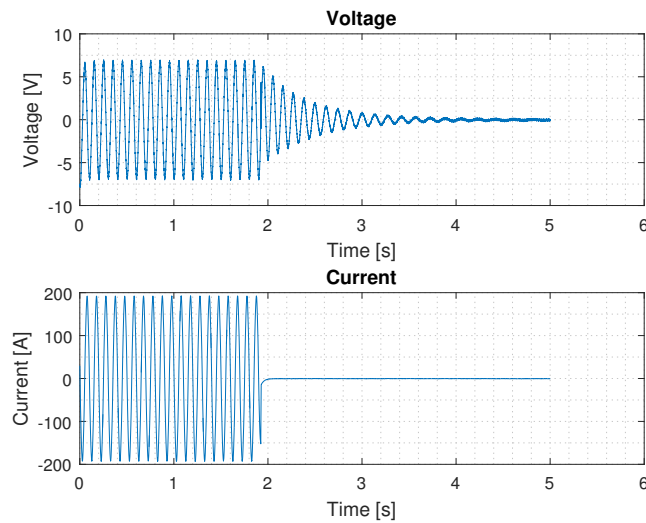

Figure 4.11: Voltage and current drop of disconnection test.

Moreover, different fitted curves are also presented in Figure 4.12, it consists of 4 different graphs at 10 Hz for different current levels.

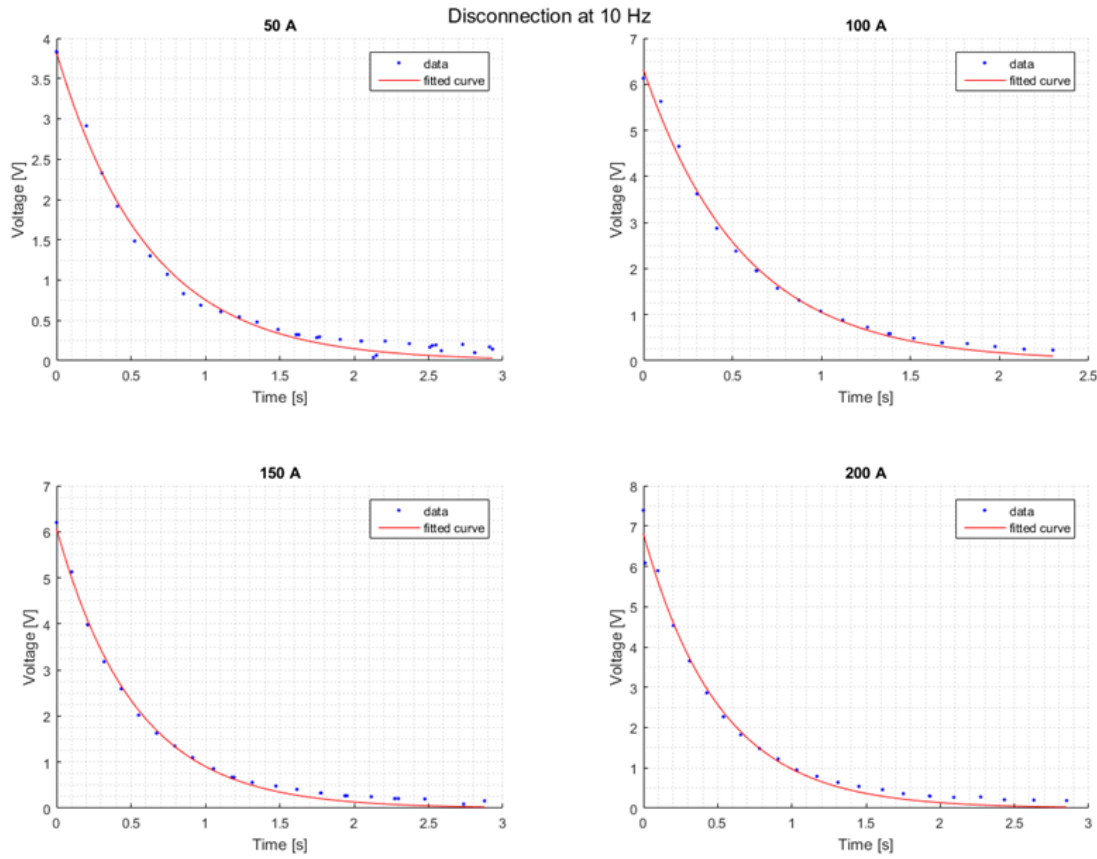**Figure 4.12:** Voltage tendency of disconnection tests at 10 Hz for machine B.

Following the disconnection calculation described in (3.1.4), the values of the rotor resistance are calculated and presented in Figure 4.13.
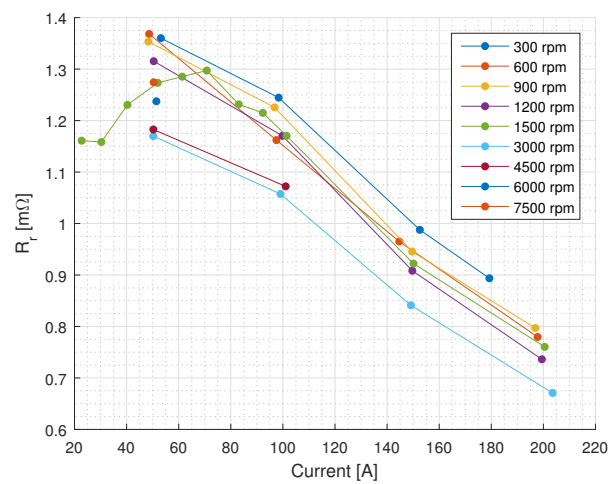

Figure 4.13: Rotor resistance of machine B calculated at different disconnection speeds.

As can be noticed, for 50 Hz more values were available at low current. The rotor

resistance was expected to be frequency dependant and fairly current independent. The values obtained are enclosed between a big gap with a lower value of 0,7 $m\Omega$ and an upper of 1,4 $m\Omega$. The reason for this behaviour is unknown.

4.1.5 Inertia

First of all, the electromagnetic torque is calculated at the instant before the disconnection subtracting 10% of the iron losses to represent the drop in flux level and all of the stator copper losses. The slip is assumed to be 0. Then, the same happens with electromagnetic power that it is calculated assuming a synchronous speed as well.
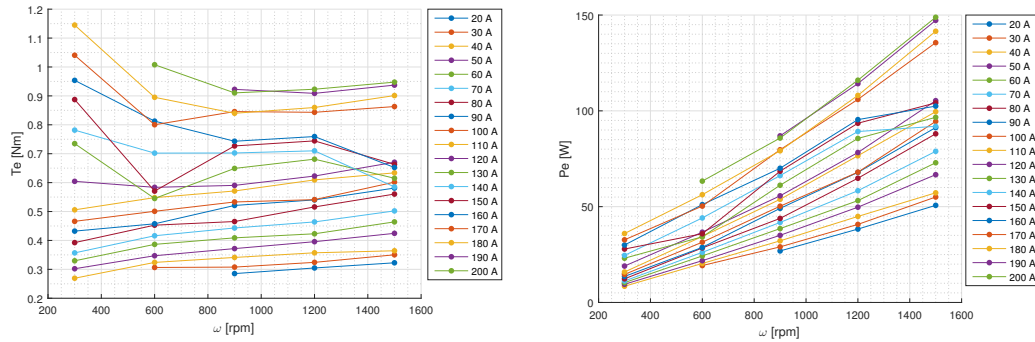
(a) Electromagnetic torque calculated for machine B at low speed rotations.

(b) Electromagnetic power calculated for low machine rotations.

Figure 4.14: Electromagnetic torque and electromagnetic power calculated from measurements at the disconnection instant of machine B.

With this measurement range a tendency can be observed. For the electromagnetic torque, it seems to be only current dependant. For low rotation speeds, values have a tendency but for upper values the results are more unpredictable. The electromagnetic power has a clear increasing tendency.

With a PLL, the change of the frequency can be studied along the time starting at the disconnection point and in this way find the speed of the machine. Then, derivative of ω over time can be calculated for different currents and initial rotation speeds.
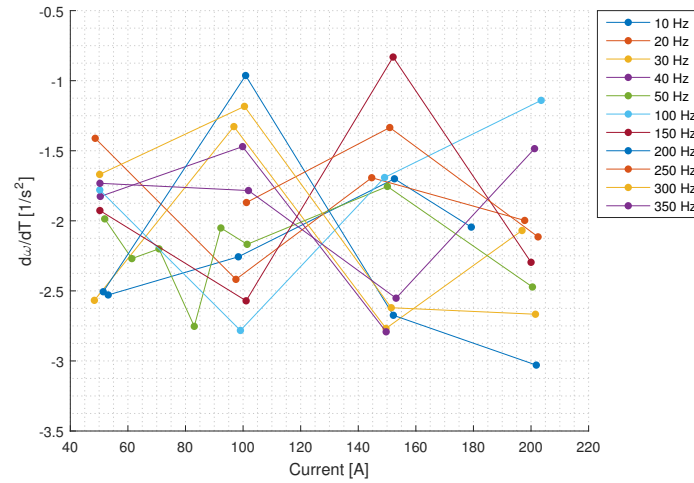
Figure 4.15: Variety of angular frequency over the current while voltage drop for machine B.

For different current starting point scenarios and different starting frequencies, the inertia can be found as explained in section 3.1.5.
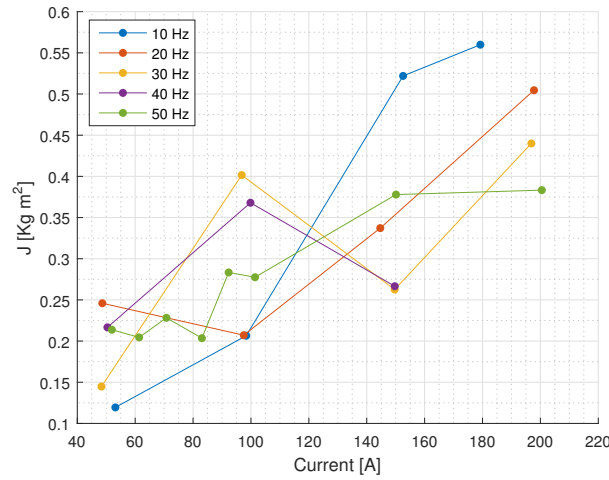
Figure 4.16: Inertia of induction machine plus gearbox calculated from machine B measurements.

Although the value should be constant for all frequencies, an enclosed area can be observed between 0,11 kgm^2 and 0,23 kgm^2 with a mean of 0,16 kgm^2 including the gearbox, despite some anomalies, especially at 10 Hz.

4.2 Machine A MotorCAD Analysis

Different calculations were done to compare the experimental results in order to validate the model. A locked rotor, single load point, no load test, breakdown test

and torque characteristic were done using the program. For the rated-load operation parameters were as shown in Table 4.4.

Table 4.4: Values for rated-load operating point.

Drive Mode	Motor
Shaft Speed	965 rpm
Slip	0,035
Frequency	50 Hz
Supply Definition	AC Mains
RMS Voltage	400 V
Winding Connection	Star
Skew of Rotor	0

Moreover, only electromagnetic results were calculated. Hence, temperatures were given to the model. Otherwise, these would have been calculated automatically with the thermal model integrated into the software. The temperatures were set as presented in Table 4.5.

Table 4.5: Temperatures definition for different machine points.

Position	Value
Winding	20 °C
Bars	20 °C
End ring	20 °C
Stator Lamination	20 °C
Rotor Lamination	20 °C
Shaft	20 °C
Wedge	20 °C

4.2.1 Equivalent Circuit

The equivalent circuit parameters for one phase of the model obtained from the analytic results are as shown in Table 4.6.

Table 4.6: Equivalent circuit parameters obtained from MotorCAD simulations and reference values for Machine A.

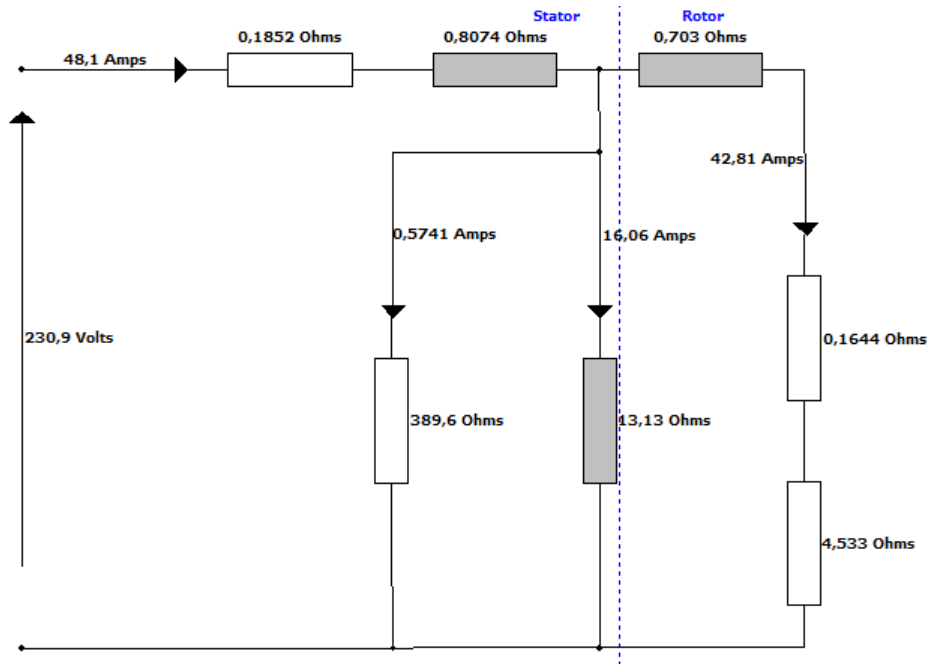| Equivalent circuit model		
Parameter	MotorCAD Simulation (Ω)	Reference (Ω)
Stator resistance	0,1852	0,18
Stator leakage reactance	0,8074	0,8
Rotor resistance	0,1644	0,19
Rotor leakage reactance	0,703	0,65
Core losses resistance	389,6	166
Magnetizing reactance	13,13	12,6

Figure 4.17: Equivalent circuit obtained with MotorCAD for machine A.

The current for the no-load test obtained from MotorCAD is 17,78 A. The results obtained from the model in MotorCAD matched the data sheet values regarding the stator, rotor and magnetizing values. Despite this, the core losses value obtained from MotorCAD is more than 2 times higher than the value obtained from the measurements and from the data sheet. By doing a Finite Element Analysis with MotorCAD, a more accurate value for core losses can be obtained. The analysis is done under no load conditions, therefore synchronous speed of the rotor is assumed. The value obtained is 223,4 Ω. The value still does not represent machine for unknown reasons. [2] [3] Puncing effects of the stator lamination can be one reason.

Moreover, simulations were repeated using the values for the material properties obtained with measurements according to [7]. Therefore, higher frequencies were added to the model losses. However, the results obtained were the same.

4.2.2 Efficiency Map

Once all the parameters have been obtained through the software and the model has been validated it, a contour plot of the efficiency of the machine can be done. This is shown in Figure 4.18
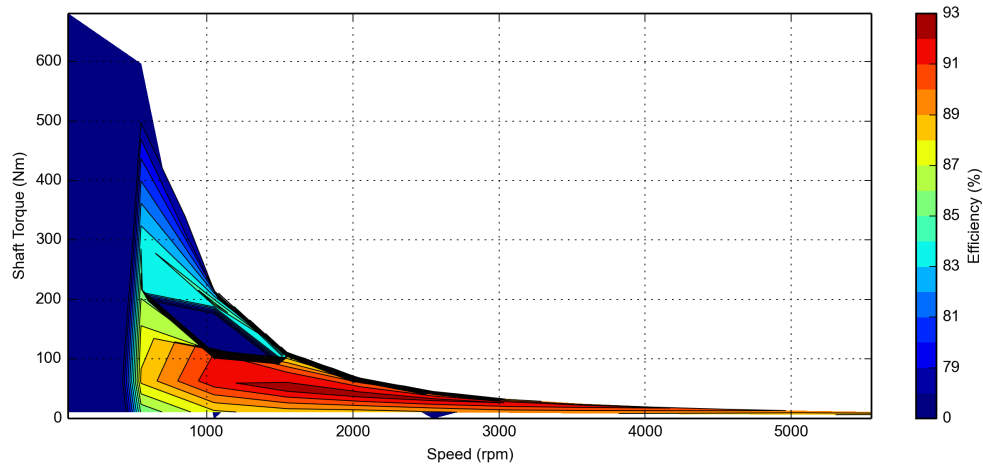
Figure 4.18: Efficiency map of machine A obtained from MotorCAD.

It can be seen how at the rated speed machine does not achieve the maximum efficiency, but for the 32 A rated current, efficiency is up to 91 %.

4.3 Machine B MotorCAD Analysis

Different tests were carried out with MotorCAD software to obtain all the parameters.

4.3.1 Stator Resistance

In order to obtain stator resistance, as it is a constant value under all conditions, a singular point shown in Table 4.7 is studied.

Table 4.7: Values set for the operating point.

Drive Mode	Motor
Shaft Speed	1500 rpm
Frequency	50 Hz
Supply Definition	AC Mains
RMS Voltage	10 V
Winding Connection	Star

Moreover, for the first model, only electromagnetic results were calculated. Hence, temperatures were given to the model. Otherwise, these would have been calculated automatically with the thermal model integrated into the software. Temperatures were estimated as shown in Table 4.8.

Table 4.8: Temperatures definition for different motor points.

Position	Value
Winding	20 °C
Bars	20 °C
End ring	20 °C
Stator Lamination	20 °C
Rotor Lamination	20 °C
Shaft	20 °C
Wedge	20 °C

The equivalent circuit parameters of the machine B obtained from the simulations are shown in Table 4.9.

Table 4.9: Equivalent circuit parameters obtained from MotorCAD for machine B under specified conditions determined for measurements.

Equivalent circuit model	
Parameter	Value
Stator resistance	0,002994 Ω
Stator leakage reactance	0,002298 Ω
Rotor resistance	0,000813 Ω
Rotor leakage reactance	0,03984 Ω
Core losses resistance	14,88 Ω
Magnetizing reactance	0,259 Ω

As can be seen, the stator resistance matches with the value obtained through the experiments and it is better than with the previous estimation done in section 3.3.1.2. That suggests that for this configuration, the winding pattern and length of the wires and the motor seems to be correct.

4.3.2 Blocked Rotor

Under blocked rotor circumstances, a wide range of frequencies and voltages were studied. Showing the following results to validate the model with the previous experiments. The graphs in Figure 4.19 show the blocked rotor resistance obtained from the simulations of the machine and a comparison of the measurements and the simulations done by MotorCAD. It uses 2 different currents to represent the increase of the resistance for all the frequencies for the measurements and the simulations.
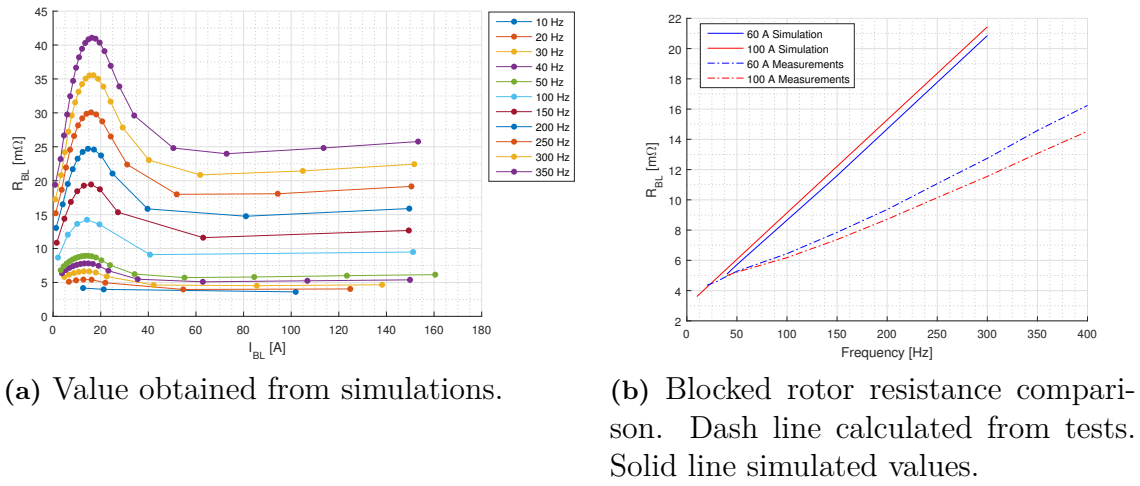
(a) Value obtained from simulations.

(b) Blocked rotor resistance comparison. Dash line calculated from tests. Solid line simulated values.

Figure 4.19: Blocked rotor resistance for machine B.

For the blocked rotor resistance, the values are quite similar for the low frequencies, but as can be seen, the values obtained from the simulations increase more for high frequencies than the results from the measurements.

The leakage inductance calculated from the simulations is shown in Figure 4.20. A comparison between the measurements and the simulations is shown as well.

(a) Blocked rotor leakage inductance from simulations for machine B.

(b) Blocked rotor inductance at 50 Hz. Dash line calculated from tests. Solid line simulated values.
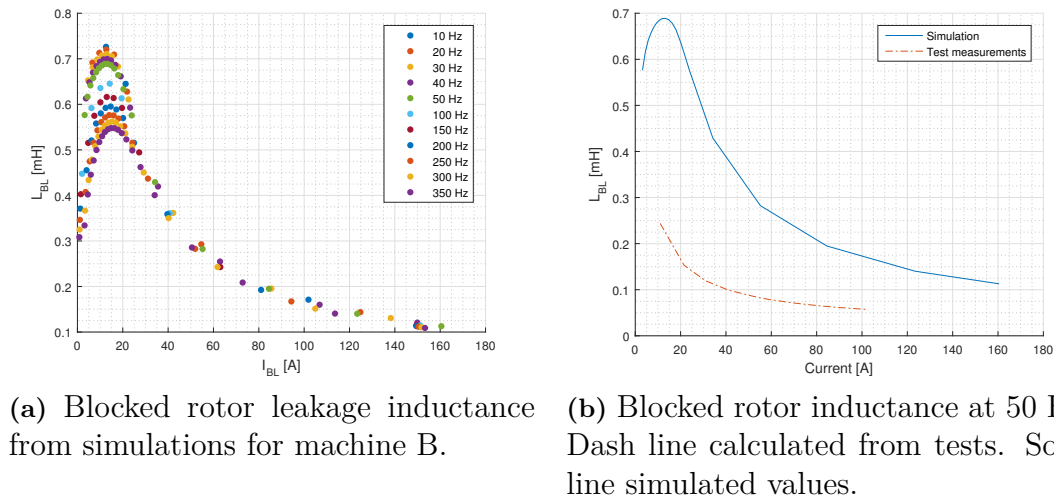
Figure 4.20: Blocked rotor inductance for machine B.

As can be seen, the values are quite different. When the simulated machine is at the maximum inductance level, the difference is maximum and around 0,45 mH. Accordingly to the test simulations seem to be about a factor of 3 higher.

4.3.3 No Load

No load tests were made to validate the model as well. First graph shown in Figure 4.21 is the no load inductance over the current and a comparison between the measurements done to machine B and the simulations from MotorCAD.
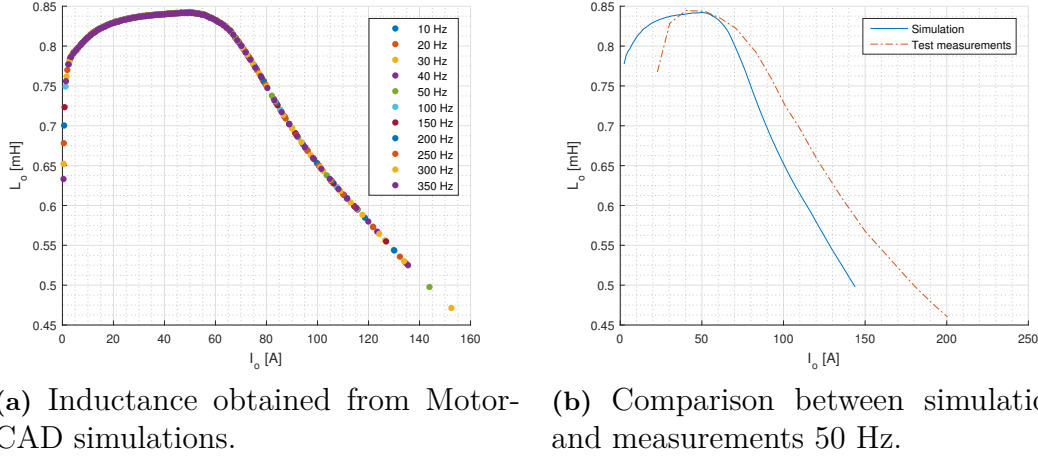

(a) Inductance obtained from Motor-CAD simulations.

(b) Comparison between simulations and measurements 50 Hz.

Figure 4.21: No load inductance for machine B using MotorCAD and measured results.

As can be observed, the values from the simulation are slightly higher for really low currents, but this is due to the fact that curve appears to be displaced. From 70 A to the upper currents, the simulated values are lower and the difference increases with the current, what means that the shape of the curves are different, having a higher slope than the one from the simulations.

In Figure 4.22 the powers are shown to compare with the measurements of the machine B. No load power for low frequencies is shown more in detail to compare with the good results obtained from the measurements.
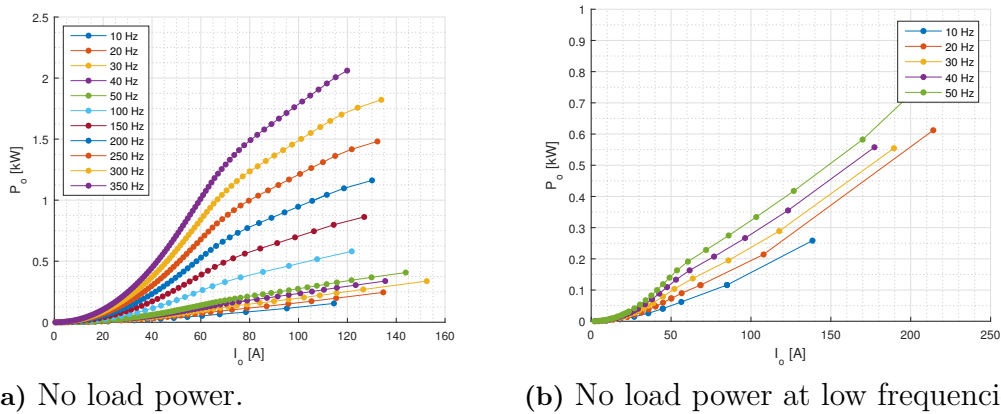

(a) No load power.

(b) No load power at low frequencies.

Figure 4.22: No load power consumption from simulations with MotorCAD for machine B.

Similarly as it has been done before, the graph in Figure 4.23 compares the input power for different scenarios between simulations and measurements.
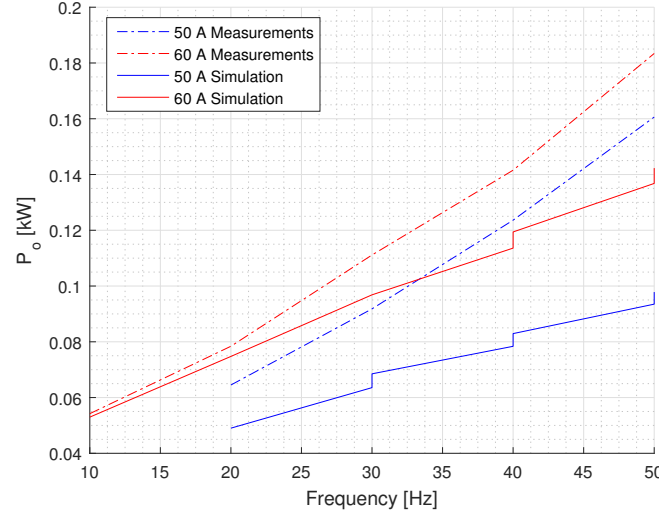
Figure 4.23: No load power. Dash line calculated from tests. Solid line simulated values with MotorCAD.

The values obtained from the simulations are as the values from the measurements. The lines do not have the same slope for low currents but the difference is only 50 W.

The same is done with the rotational losses, where they are plotted over the no load current in Figure 4.24. A comparison between the measurements and the simulations is added for a better understanding.
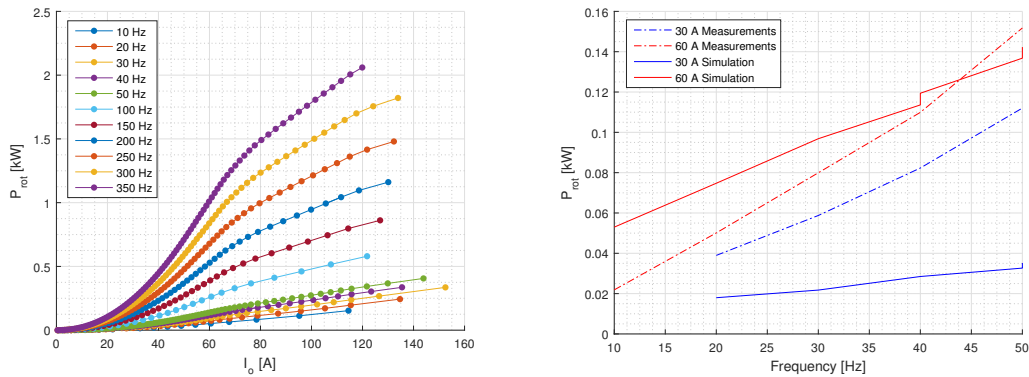
(a) Rotational power for on load test from simulations for machine B.

(b) Rotational losses for different current levels. Dash line calculated from tests. Solid line simulated values with MotorCAD.

Figure 4.24: Rotational power losses from machine B.

The values are similar , with a maximum difference of 60 W for 30 A. Moreover, the rotor resistance over the no load current is shown below. It can be observed how the skin effect works for high frequencies and how it should be current independent. The obtained value from simulations is a factor of 3 bigger than measurements for unknown reasons.
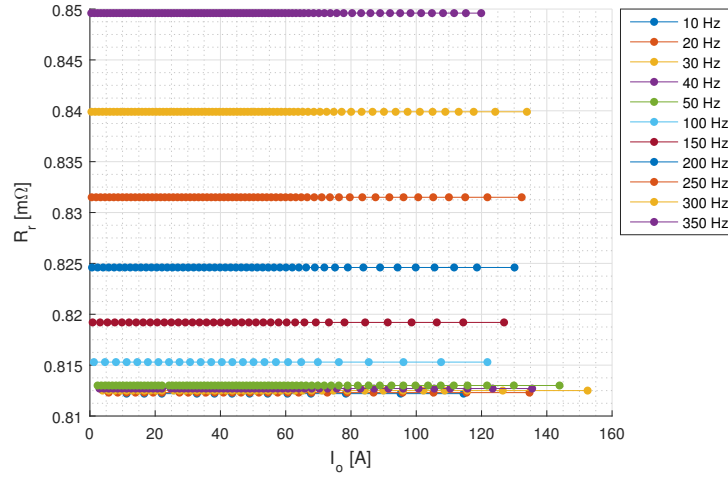
Figure 4.25: Rotor resistance from simulations of machine B.

After analyzing all the parameters obtained from the simulations and comparing them with the values obtained from the measurements done on the real machine, it can be said that model works fairly properly under certain circumstances.

4.4   Maxwell Analysis of Machine A and B

Machine A and B are modeled in Maxwell to simulate the no load test and locked rotor test to obtain the equivalent circuit parameters. Then the simulation result is compared with actual test results obtained previously [2] [3].

4.5   Comparison of Parameters

4.5.1   Machine A

Result from Maxwell simulation [8] with a stator resistance without end winding of 0.099 Ω, matching the value got from manual calculation. With addition of end winding the resistance becomes 0.19 Ω. No-load inductance at 50 Hz was found to be 43.3 mH, 5% higher than the measured value. Iron loss resistance was found to be 253 Ω, which is 5% below the measured value. In figure 4.26, the magnetizing inductance of Machine A is presented.
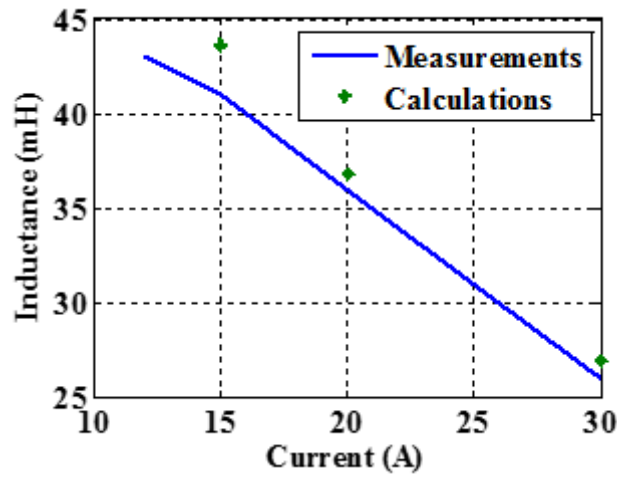
Figure 4.26: Measured and calculated magnetizing inductance of Machine A.

For the locked rotor test, the locked rotor inductance was found to be 1 mH lower than the previous measurements as shown in figure 4.27.
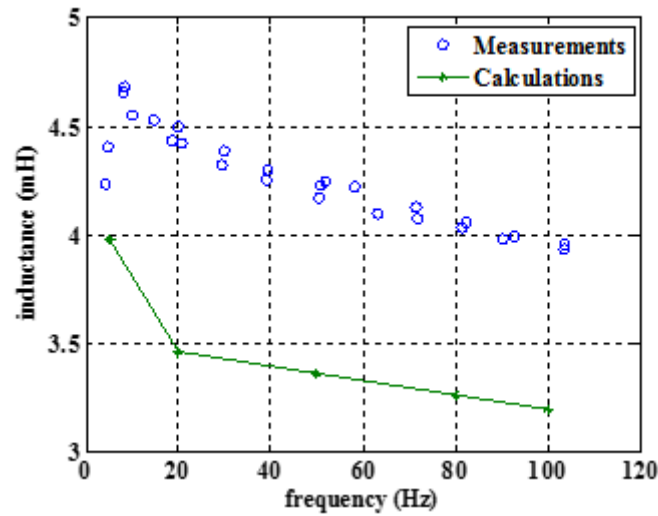
Figure 4.27: Measured and calculated locked rotor inductance of Machine A at 20 A current.

The calculated locked rotor resistance was also found to be a bit lower than the measurements as shown in figure 4.27. The impact of skin effect is bit lower from calculated values. This is confirmed by comparing the measured and calculated torque values as presented in figure 4.29.

The calculated locked rotor inductance and locked rotor resistance is found to be 20 % below at 50 Hz. The resistance discrepancy observed to be increasing with increase of frequency.

Figure 4.28: Measured and calculated locked rotor resistance of Machine A at 20 A current.
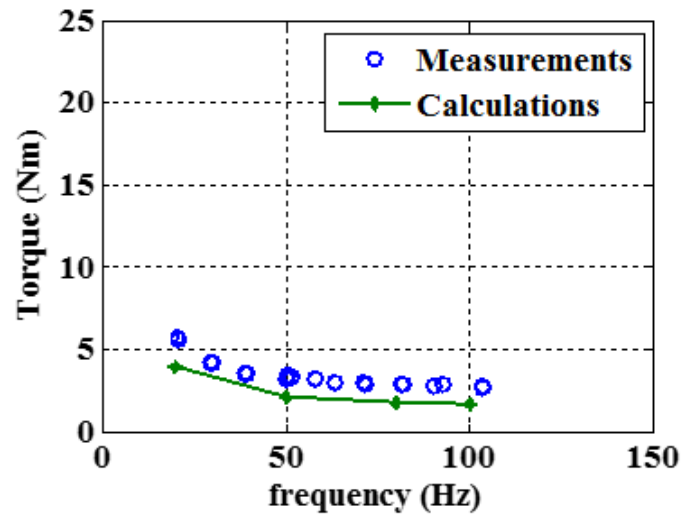
Figure 4.29: Measured and calculated torque of Machine A at 20 A current.

4.5.2   Machine B

Results shown in tables 4.10 and 4.11 shows comparative values of the equivalent circuit parameters.

Table 4.10: Comparative no load results output for machine B at 70 A and 50 Hz.

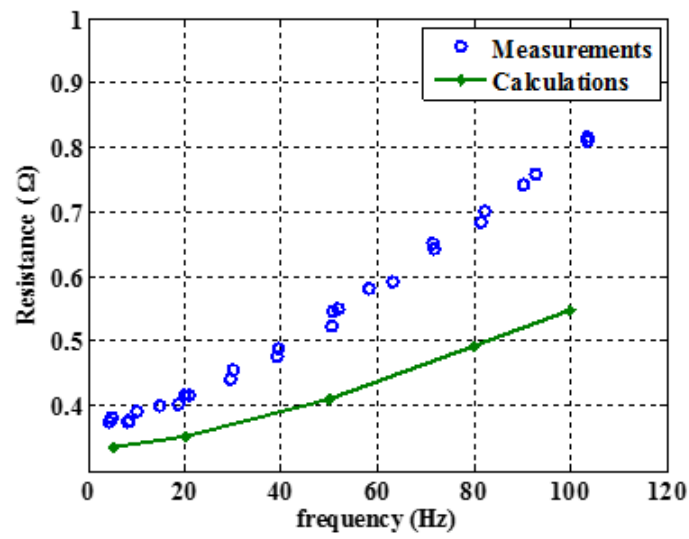| No Load Results for Machine B at 70A at 50 Hz			
Parameter	Maxwell	MotorCAD	Measurement
Stator resistance(Ω)	0,003288	0,002994	0,0028
R_{NL} (Ω)	0,005	0,00744	0,004775
X_{NL} (Ω)	0,232	0,250845	0,257517

Table 4.11: Comparative locked rotor results output for machine B at 120 A at 100 Hz.

Locked rotor Results for Machine B at 120 A and 100 Hz			
Parameter	Maxwell	MotorCAD	Measurement
R_{BL} ($m\Omega$)	6,1	9,5	5,2
X_{BL} ($m\Omega$)	37,7	87,9	31,2

From tables 4.10 and 4.11, the output values of R_{NL}, X_{NL}, R_{BL} and X_{BL} from Maxwell are matching with measurement values. The values obtained under blocked rotor conditions differ less than the values under no load conditions. The output values of X_{NL} from MotorCAD match with the measurements better than the result from Maxwell while the value of R_{NL} from MotorCAD differs more. Under no load conditions, the MotorCAD outputs X_{BL} and R_{BL} are not matching with the measurement value. The reason for this is unknown.
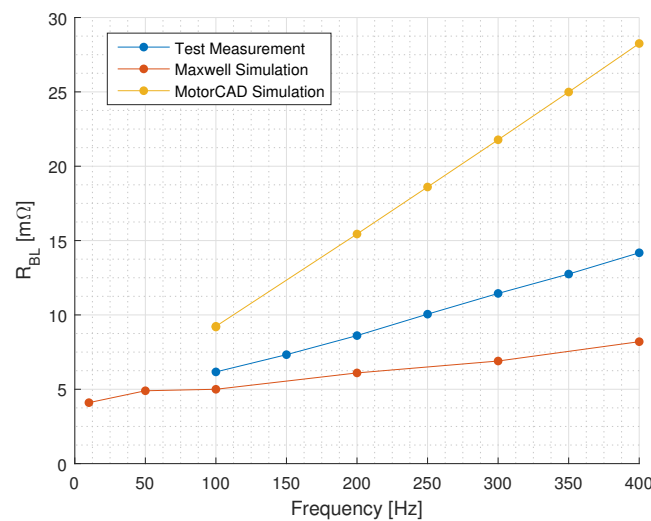
Figure 4.30: Blocked rotor resistance obtained from test measurements, simulations with MotorCAD and Maxwell software at 120 A.
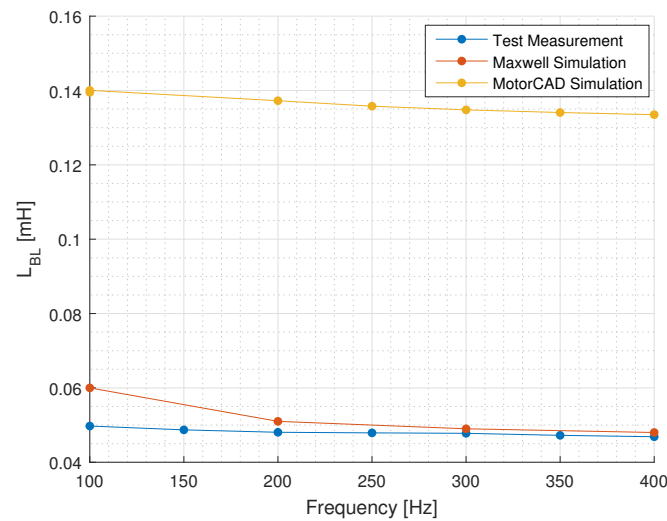
Figure 4.31: Blocked rotor inductance obtained from measurements, simulations with MotorCAD and Maxwell software at 120 A.

A comparative figure is plotted in Figure 4.30 for blocked rotor resistance and blocked rotor inductance in Figure 4.31. It can be observed that the test measurements and Maxwell values match for the blocked rotor resistance for low frequencies, whereas the measurements and Maxwell results for blocked rotor inductance tends to converge for higher frequencies better than MotorCAD. The Maxwell simulation results are plotted along with measurements for magnetizing inductance [8] in Figure 4.32. The results tends to follow the same trajectory.
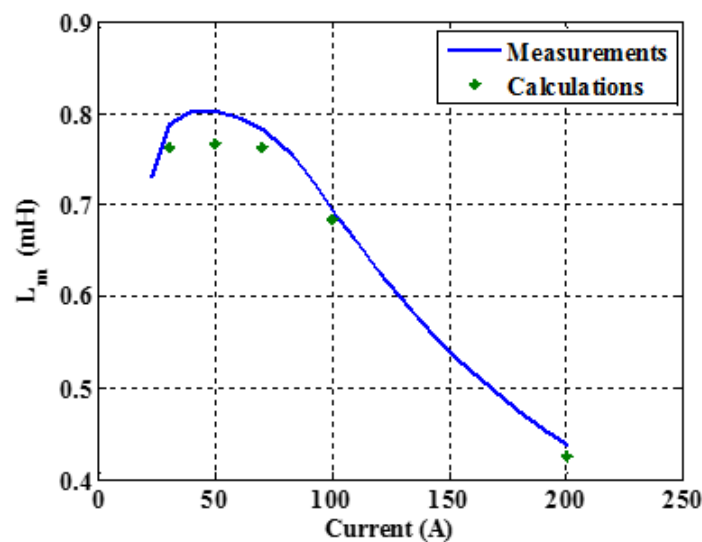
Figure 4.32: Magnetizing inductance of Machine B as a function of magnetizing current.

5

Conclusions

5.1 Results

First of all, a characterization of machine B, the one that is being used currently in some cars, has been conducted. Even though that for some current and frequency levels it was not possible to get good results for the locked-rotor case, for a wide range of working points the results appeared to be good.

For machine A, a good model was set up in both software, Maxwell and MotorCAD, that allowed an electrical simulation of these machines. With this model, it was easy to understand how both software programs work and how they do the calculations. With this knowledge, it was easier to set up a model for machine B. The model for machine B was not perfectly working in the two software programs, as some parameters like the rotor resistance differ from the measurements done. Specifically in the model of machine B in MotorCAD, the blocked rotor inductance was more than two times bigger. For the blocked rotor resistance, the value obtained with MotorCAD increases more with the frequency than the measurements and with the values obtained using Maxwell. The reason for this is unknown. Despite this, a model for this machine has been set that can simulate the no-load behaviour of the machine with the two software.

5.2 Future Work

First of all, the model problems should be solved, and if the problems remain, the software suppliers could be contacted.

As a future extension of this thesis work, it would be interesting to do more measurements of machine B for high frequencies and currents to understand properly its behaviour on this area. More simulations and testing comparisons could be done as well in other working points of the machine. Furthermore, a proper measurement of the wire diameter of the windings of machine B could be done, as well as a deeper study of the winding pattern to assure that it is as described on this thesis.

It is known that all the electric conductors change their properties under thermal effects, as the resistivity is not a constant value, and among some parameters, it depends on the temperature. For this reason, it would be interesting to set up a model that takes these effects into account. It might be that with this model, the parameters of machine B could better fit the measurements done in this thesis. By

doing this, not only better results would be achieved, but also a better understanding of the machine and the losses will be given.

The machine B model in MotorCAD can be analyzed more to find out the reason behind the mismatch of the values of R_{BL} and L_{BL} with the measurement values.

Moreover, it would be interesting as well to work further on the development of machine B. As it is a motor being used currently on cars, with the model, some different changes can be done to the geometry, winding, materials, etc. And according to real constructive possibilities, a better machine can be created that minimizes actual losses.

Bibliography

[1] T. MIT. (2016). The future of strategic natural resources, [Online]. Available: `http://web.mit.edu/12.000/www/m2016/finalwebsite/about.html` (visited on 04/26/2017).

[2] T. Thiringer, "Measurements and modelling of low-frequency disturbances in induction machines", PhD thesis, Chalmers University of Technology, 1996.

[3] G. Kylander, "Thermal modelling of small cage induction motors", PhD thesis, Chalmers University of Technology, 1995.

[4] F. I. AHMED and I. A. M. ABDEL-HALIM, "Exact analytical solution of induction motor equations following supply disconnection", *Electric Machines & Power Systems*, vol. 5, no. 4, pp. 323–330, 1980. DOI: `10.1080/07313568008955413`. eprint: `http://dx.doi.org/10.1080/07313568008955413`. [Online]. Available: `http://dx.doi.org/10.1080/07313568008955413`.

[5] "Ieee recommended practice for electric power distribution for industrial plants", *IEEE Std 141-1993*, pp. 1–768, Apr. 1994. DOI: `10.1109/IEEESTD.1994.121642`.

[6] J. M.-T. B. Despalatović M., "Identification of induction motor parameters from free acceleration and deceleration tests", *Automatika : časopis za automatiku, mjerenje, elektroniku, računarstvo i komunikacije*, 2005.

[7] O. Aglén, "Mätning av järnförluster vid höga frekvenser", PhD thesis, Kungl Tekniska Högskolan, 1991.

[8] A. R. Torbjörn Thiringer, "Investigation of a traction induction machine through student works", Swedish Electromobility Centre, 2017.

A

Appendix 1

A.1   Material Properties

Table A.1: Material data.

Material	Used in	Resistivity (Ωm)	Density (kg/m^3)
Copper die cast	A and B windings, B rotor cage	1,68E-8	8933
Aluminium cast	A rotor cage	3,3E-8	2950
M700-50A	A rotor and stator laminations	2,5E-7	7872
M235-35A	B rotor and stator laminations	5,9E-7	7600

A.1.1   M700-50A

Table A.2: Magnetization values used for M700-50A.

B [T]	H [A/m]
0	0
0.1	67.8
0.2	88.3
0.3	99.2
0.4	108
0.5	116
0.6	124
0.7	132
0.8	142
0.9	152
1	164
1.1	180
1.2	206
1.3	254
1.4	363
1.5	690
1.6	1760
1.7	4230
1.8	8130
1.8027578	8239.62478
1.810511	8571.8637
1.8219167	9137.3497
1.8353172	9955.8139
1.8492444	11060.024
1.8627151	12504
1.8753024	14381.696
1.8871165	16878
1.8989856	20467.088
1.9193255	30000
3,8	1584158

For the losses model, following data was used for M700-50A steel.

II

Table A.3: Steel losses of M700-50A.

Frequency [Hz]	Loss Density [kW/kg]	Flux Density [T]
50	5E-5	0,1
50	0,00016	0,2
50	0,00037	0,3
50	0,00059	0,4
50	0,00084	0,5
50	0,00112	0,6
50	0,00143	0,7
50	0,00177	0,8
50	0,00215	0,9
50	0,00257	1
50	0,00303	1,1
50	0,00355	1,2
50	0,00413	1,3
50	0,00483	1,4
50	0,00569	1,5
50	0,00654	1,6
50	0,00729	1,7
50	0,00781	1,8

A.1.2   M235-35A

Table A.4: Magnetization values used for M235-35A.

B [T]	H [A/m]
0	0
0,1	24,7
0,2	32,6
0,3	38,1
0,4	43,1
0,5	48,2
0,6	53,9
0,7	60,7
0,8	68,8
0,9	79,3
1	93,7
1,1	115
1,2	156
1,3	260
1,4	690
1,5	1950
1,7	7630
1,8	12000
3,8	1584158

For the losses model, following data was used for M235-35A steel.

Table A.5: Steel losses of M235-35A at 50 Hz.

Frequency [Hz]	Loss Density [W/kg]	Flux Density [T]
50	0	0
50	0,02	0,1
50	0,06	0,2
50	0,11	0,3
50	0,2	0,4
50	0,29	0,5
50	0,38	0,6
50	0,5	0,7
50	0,62	0,8
50	0,77	0,9
50	0,92	1
50	1,1	1,1
50	1,31	1,2
50	1,56	1,3
50	1,92	1,4
50	2,25	1,5
50	2,53	1,6
50	2,75	1,7
50	2,94	1,8

Table A.6: Steel losses of M235-35A at 100 Hz.

Frequency [Hz]	Loss Density [W/kg]	Flux Density [T]
100	0,04	0,1
100	0,14	0,2
100	0,3	0,3
100	0,49	0,4
100	0,71	0,5
100	0,97	0,6
100	1,25	0,7
100	1,57	0,8
100	1,92	0,9
100	2,31	1
100	2,75	1,1
100	3,26	1,2
100	3,88	1,3
100	4,67	1,4
100	5,54	1,5

Table A.7: Steel losses of M235-35A at 200 Hz.

Frequency [Hz]	Loss Density [W/kg]	Flux Density [T]
200	0,08	0,1
200	0,32	0,2
200	0,73	0,3
200	1,21	0,4
200	1,78	0,5
200	2,44	0,6
200	3,19	0,7
200	4,03	0,8
200	4,97	0,9
200	6,01	1
200	7,19	1,1
200	8,54	1,2
200	10,1	1,3
200	12,2	1,4
200	14,4	1,5

Table A.8: Steel losses of M235-35A at 400 Hz.

Frequency [Hz]	Loss Density [W/kg]	Flux Density [T]
400	0,19	0,1
400	0,87	0,2
400	1,88	0,3
400	3,17	0,4
400	4,73	0,5
400	6,56	0,6
400	8,67	0,7
400	11	0,8
400	13,8	0,9
400	16,9	1
400	20,3	1,1
400	24,3	1,2
400	28,9	1,3
400	34,8	1,4
400	41,2	1,5

Table A.9: Steel losses of M235-35A at 1000 Hz.

Frequency [Hz]	Loss Density [W/kg]	Flux Density [T]
1000	0,93	0,1
1000	3,55	0,2
1000	7,45	0,3
1000	12,3	0,4
1000	18,5	0,5
1000	25,8	0,6
1000	34,6	0,7
1000	45	0,8
1000	57,2	0,9
1000	71,5	1
1000	88,3	1,1

Table A.10: Steel losses of M235-35A at 2500 Hz.

Frequency [Hz]	Loss Density [W/kg]	Flux Density [T]
2500	3,89	0,1
2500	14,3	0,2
2500	29,6	0,3
2500	50,2	0,4
2500	76,7	0,5
2500	110	0,6
2500	153	0,7
2500	205	0,8
2500	270	0,9
2500	349	1

A.2 Study of the Effect of the End Ring Geometry

It is interesting to study the effect of end ring impedance on the machine A. As for Maxwell software this values has to be introduced directly, with MotorCAD, can be calculated by changing the geometry. A study of its sensitivity is done with MotorCAD for 15 kW machine configuration.

Table A.11: Effect of end ring on 15 kW machine.

EndRing Thickness (mm)	Inductance (mH)	Resistance (Ω)
1	8,595E-005	2,595E-005
15	6,617E-005	1,73E-006
30	5,491E-005	8,65E-007

Resistance decreases whilst thickness increases as expected. Inductance values decreases as well.